AD-A156 639 HIGH TEMPERATURE MECHANICAL TESTING OF A CYLINDRICAL WEAVE CARBON-CARBON..(U) CALIFORNIA UNIV LOS ANGELES SCHOOL OF ENGINEERING AND APPLIED.. S MACK ET AL. 1/1

UNCLASSIFIED 01 JUL 85 UCLA-ENG-85-20 N00014-77-C-0505 F/G 11/4 NL

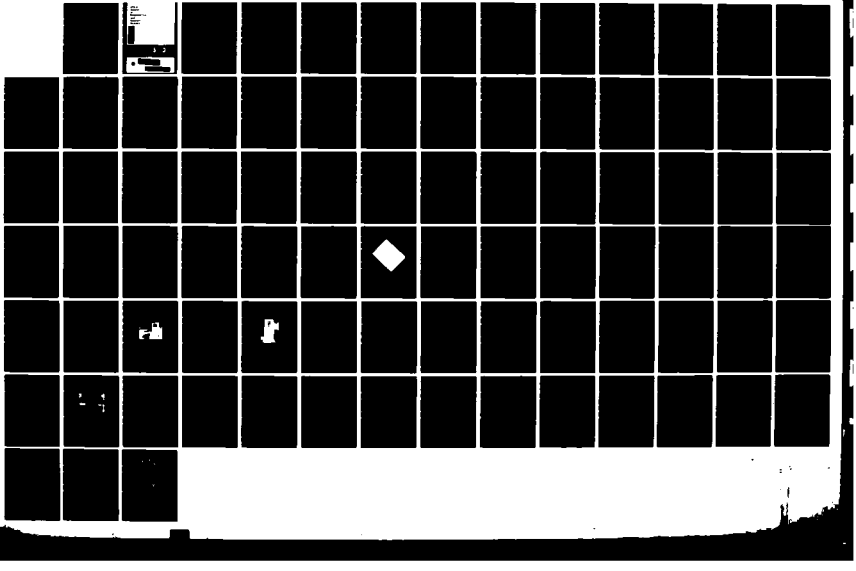

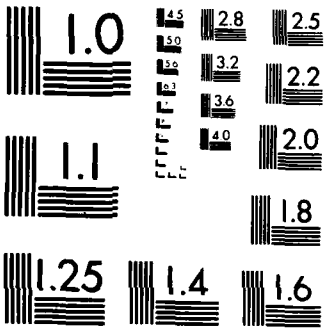

UCLA School of Engineering and Applied Science

HIGH TEMPERATURE MECHANICAL TESTING OF A CYLINDRICAL WEAVE CARBON-CARBON COMPOSITE

by Steven Mack and George Sines

ONR-N0014-77-C-0505
L.H. Peebles, Monitor

UCLA-ENG-85-20
July 1985

SECURITY CLASSIFICATION OF THIS PAGE (When Data Entered)

REPORT DOCUMENTATION PAGE		READ INSTRUCTIONS BEFORE COMPLETING FORM
1. REPORT NUMBER	2. GOVT ACCESSION NO. AD-A156 639	3. RECIPIENT'S CATALOG NUMBER
4. TITLE (and Subtitle) High Temperature Mechanical Testing of a Cylindrical Weave Carbon-Carbon Composite		5. TYPE OF REPORT & PERIOD COVERED Technical Report
		6. PERFORMING ORG. REPORT NUMBER UCLA-ENG-85-20
7. AUTHOR(s) Steven Mack and George Sines		8. CONTRACT OR GRANT NUMBER(s) N0014-77-C-0505
9. PERFORMING ORGANIZATION NAME AND ADDRESS School of Engineering and Applied Science University of California Los Angeles, CA 90024		10. PROGRAM ELEMENT, PROJECT, TASK AREA & WORK UNIT NUMBERS
11. CONTROLLING OFFICE NAME AND ADDRESS Office of Naval Research Att. Dr. A.M. Diness Arlington, Virginia 22217		12. REPORT DATE 1 July 85
		13. NUMBER OF PAGES 81
14. MONITORING AGENCY NAME & ADDRESS(if different from Controlling Office) Monitor, Dr. L.H. Peebles, Jr. Office of Naval Research Arlington, Virginia 22217		15. SECURITY CLASS. (of this report) Unclassified
		15a. DECLASSIFICATION/DOWNGRADING SCHEDULE
16. DISTRIBUTION STATEMENT (of this Report) Unlimited		
17. DISTRIBUTION STATEMENT (of the abstract entered in Block 20, if different from Report)		
18. SUPPLEMENTARY NOTES		
19. KEY WORDS (Continue on reverse side if necessary and identify by block number) Carbon-Carbon Composites; Graphite; Shear-Lag; Rocket Nozzles; Fabrication Stresses		

20. ABSTRACT (Continue on reverse side if necessary and identify by block number)

The goal is to provide the material property information that is needed to decide whether radial bundles can reduce the stress in the circumferential bundles during the thermal processing of billets. Testing consisted of bundle pull-out experiments at room, 1000C, and 1500C on coupons excised from a billet and of rupture and creep experiments on bundles processed to different degrees.

DD FORM 1 JAN 73 1473 EDITION OF 1 NOV 65 IS OBSOLETE
S/N 0102 LF 014 6601

SECURITY CLASSIFICATION OF THIS PAGE (When Data Entered)

The pull-out specimens showed increasing shear strength with temperature and the data showed a decrease in the coefficient of variation with temperature. The average bundle-matrix bond strength at 1500C had a value of 1940 ksi with a coefficient of variation of 4.9%. The tests at 1000C and room temperature had a coefficient of variation of 7.9% and 19.2% respectively. The tensile strengths of the bundles were relatively insensitive to processing and varied from 190 to 260 ksi. No creep was observed at the maximum available temperature of 1800C.

TABLE OF CONTENTS

LIST OF TABLES

LIST OF FIGURES

NOMENCLATURE

C = Circumference of Billet

R = Radius of Billet

ϵ = Creep Strain

ϵ_m = Matrix Strain

t = Time

T = Temperature

F = Force

Z = Axial Direction

θ = Circumferential Direction

r = Radial Direction

SUBSCRIPTS

o = Outer

i = Inner

$\theta\theta$ = Circumferential Surface, Circumferential Direction

rr = Radial Plane, Radial Direction

zz = Axial Plane, Axial Direction

f = Fiber Bundle

m = Matrix

ABSTRACT

High Temperature Mechanical Testing
of a Cylindrical Weave Carbon-Carbon Composite

The purpose is to help decide whether the radial fibers in a cylindrical weave carbon-carbon composite can relieve the circumferential stress prevalent during the high temperature processing of composite billets. Included in this report are data from high temperature mechanical testing in temperatures in excess of 1800 C. This testing includes pull-out experiments of coupons taken directly from a Navy billet given to us some time ago, specifically pulling both the axial and radial fiber bundles from the composite matrix at temperatures of room, 1000 C and 1500 C. Also included are tests on axial rupture, and creep of in-house processed, impregnated, and graphitized fiber bundles. The data taken for the creep specimens showed no elongation at a temperature of 1800 C with a stress of aproximately 11 ksi for period of 20 min.

The axial rupture specimens were processed to different degrees then tested at ambient. All these specimens failed at stresses between 190 ksi and 260 ksi. The pull-out specimens showed a curve of increasing shear strength with temperature but more important, the data taken show a decrease in the coefficient of variation of the data with temperature. The average maximum peak shear strength was recorded at 1500 C and had a value of 1940 ksi with a coefficient of variation of only 4.9%. The data for the temperatures of 1000 C and room temperature showed a considerable scatter with room temperature having a coefficient of variation of 19.2% and a coefficient of variation of 7.9% for the specimens tested at 1000 C.

1) INTRODUCTION:

During the fabrication of cylindrically woven carbon-carbon composites, large scale fractures and/or gross waviness sometimes occur in the circumferential fiber bundles. Since anomalies such as these have the effect of reducing the strength and structural integrity of the billet, the understanding of the origin of these anomalies as well as developing measures to prevent them during fabrication is essential.

These anomalies are usually caused by thermal stresses arising from the repeated heating to, and cooling from, the graphitization temperature. These stresses occur because of the anisotropy of both the thermal coefficient of expansion and the elastic moduli. One of the generally accepted functions of the radial fiber bundles is to reduce the stress in the circumferential direction by restricting the thermally induced radial expansion during heat-up, thereby reducing the probability of circumferential failure during fabrication. This reasoning has its merits; however, a simple analysis by Quan and Sines, (ref 2), in appendix A, shows that the stress in the radial direction is always greater than that in the circumferential direction. This, combined with the usually lower radial fiber volume fraction dictates that

the radial fibers should rupture or become debonded long before the circumferential fibers fracture.

Since the radial fibers terminate where the two ends of the bundles intersect the free surfaces of the billet, a zone of high shear between the bundle and matrix must exist at these terminations. If these shear stresses are greater than the bundle-matrix interfacial shear strength, the bundle will break free from the surrounding matrix so that the only tensile stress in the bundle is that resulting from loads transferred by friction and by the interlocking of disparities between the bundle and matrix. A room temperature photomicrograph of a θ-Z plane in a billet coupon, figure 1, shows cracking in the bundle-matrix interface of the radial bundle. This supports the belief that the radial fibers may do very little to reduce the circumferential stresses in the billets made by the current processing techniques. In order to fully understand the effectiveness of the radial bundles, high temperature mechanical testing is to be performed in order to answer the following questions:

1) At elevated temperatures approaching that for graphitization, does a bond still exist between the radial bundles and the rest of the composite? if so, what is its strength?

2) At elevated temperatures approaching that for

graphitization, can stress be transmitted to the radial bundle by friction and the interlocking of disparities, even if it is completely debonded? There may be friction because of the high diametral expansion of the bundles caused by the high coefficient of thermal expansion in that direction which could create a large normal force on the matrix interface.

3) If the radial stress is completely transmitted to the fibers, i.e. perfect bonding, can the bundle survive without fracture?

4) Is it possible that creep of the radial bundle can prevent both its failure, as well as the failure of the bundle-matrix interface bond?

It may be possible, if these questions are answered, that certain fabrication parameters such as: temperature, pressure, heating rate, cooling rate, and holding temperature, can be selected to maximize the effect of the radial bundles in reducing the circumferential stresses.

2 CARBON-CARBON COMPOSITE PROCESSING

2.1 MATRIX

The matrix material used in the manufacture of carbon-carbon composite billets is either a petroleum or coal tar based pitch. When heated, portions of the pitch are volatilized and condensed aromatic rings are free to form. At a temperature of approximately 350 C, the pitch enters a transition stage called mesophase. Mesophase pitch is a two phase system of ordered and disordered pitch. The anisotropic planar crystals of pitch, which are hexagonal arrays of covalently bonded carbon atoms, are called basal planes. At an early stage of growth the basal planes are randomly oriented throughout the matrix pitch. As the temperature and the molecular size increases, these localized regions of anisotropic material tend to coalesce and stack on top of each other. Bonded together only by Van der Waals forces, these planes form large regions of anisotropy within the pitch. Application of pressure and the flow of the mesophase pitch causes alignment of these anisotropic regions, thus matrix orientation can be generated and varied as a function of processing parameters.

2.2 GRAPHITE FIBERS

High strength-high modulus graphite fibers are delivered in tows or yarns of multiple filaments. Each filament is approximately 7μm and has a microstructure of "Turbostatic" graphite, one of the allotropic forms of carbon.(3) The atoms in a single crystal of graphite are arranged in hexagonal arrays called basal planes, which are stacked in layers. The carbon atoms within the basal planes are held together by very strong covalent bonds while much weaker Van der Waals forces hold the stacking layers together. Unlike the matrix material, the basal planes are highly oriented along the axis with the c-axis perpendicular to the axis of the fiber, thus resulting in the high anisotropy of carbon fibers. The higher strength and stiffness of carbon fibers is directly related to the perfection in alignment. The degree of perfection in alignment varies considerably with processing. Imperfections in alignment, as shown schematically in figure 2, result in complex shaped voids which are stress concentrators and points of weakness leading to a reduction of strength and elastic modulus.

The graphite fiber used in the navy billet and the in-house processed test specimens are made by Hercules Incorporated using the PAN process. This process uses

stretching of a polymer precursor for the alignment of carbon atoms. PAN, or "Polyacrylonitrile" is an acrylic copolymer precursor with a molecular configuration similar to that of polyethelene except that every alternate hydrogen side group is replaced by a nitrile (-C≡N) group, figure 3. A concentrated solution of molten PAN is spun into filaments then stretched to produce alignment of the molecular chains along the filament axis. The stretched filament is then heated and the "active" nitrile groups interact to produce a ladder polymer, figure 4. The strength and elastic moduli are highly dependent upon final processing temperature as shown in a characteristic plot, figure 5 (ref 3). The PAN fibers are classified as two types: Type I, processed for maximum elastic modulus, and Type II, processed for maximum strength.

3. THE BILLET AND ITS FABRICATION

The billet used in this study is designated as Navy-C4X1, three-dimensional, cylindrically woven, carbon-carbon composite. Fabrication of this billet was done by General Electric, using a multiple high-temperature, high-pressure, impregnation-graphitization process. Details of this processing and the materials used for this billet are described as follows. The graphite fibers used in the billet preform were PAN fibers fabricated by Hercules Incorporated, Magnamite Graphite Fibers Division. The matrix material is designated as CP277-15V, coal tar pitch processed by Allied Chemical Corporation. The billet preform is woven using high modulus HM-3000 yarn in the radial direction and HM-10000 in both the axial and circumferential directions. The 10000 and 3000 designate the number of filaments in each yarn. The variable fiber volume fractions are shown in figure 6, and the properties of the fiber and pitch materials are presented in tables (1) and (2) respectively.

Automatic weaving of this three-dimensionally reinforced composite billet preform, consists of fabrication and assembly of yarn bundles in the three orthogonal directions, (radial, axial, and circumferential),

the circumferential bundles are continuous, while the length of the axial and radial bundles match the billet dimensions. The preform is heated to a minimum temperature of 350 C before the impregnation and densification cycle in order to clean the fibers of any sizing used to protect the fibers during handling. During the initial impregnation, molten coal tar pitch flows into the mold containing the billet preform impregnating the fibers, as well as filling the matrix pockets. The mold is then heated through the mesophase transition temperature very slowly, to avoid percolation, and a pressure of 15 ksi is applied for densification. The last step in the initial process is graphitization. The billet is subjected to a uniform increase in temperature up to 2750 C (5000 F). At this temperature, the basal planes in the matrix material try to align themselves along the axis of the fibers. This reduction of interatomic spacing along with the thermal contraction of the matrix, which is being inhibited by the high elastic modulus and low coefficient of thermal expansion of the bundles in their axial direction during cooling, causes cracking of the matrix. These cracks are then filled during subsequent densification cycles. The densification process involves: vacuum impregnation, (the degree of which is dependent on pore size , pore size distribution, and gas permeability),

carbonization, and graphitization. This process was repeated four times for this particular billet.

4. TEST SPECIMENS

We used two main types of test specimens. The first specimen is used in uniaxial loading for both tensile rupture and creep tests. The finished specimen is shown schematically in figure 7. The second specimen is a plug cut directly from the navy billet, and is used for the pull-out experiments. An excised radial plug is shown schematically in figure 8.

4.1 PROCESSING OF AXIAL TEST SPECIMENS

Dry fiber bundles designated as HM-3000, were received from Hercules Incorporated. These fibers are then tied as shown in figure 7, using cotton string. Cotton is used because, as an organic material, it will keep its strength at elevated temperatures even when it turns into carbon. The fibers are then washed in methyl ethyl ketone to dissolve any protective sizing.

The coal tar pitch, designated as CP277-15V is produced by Allied Chemical Corporation. The pitch is preheated to a maximum temperature of 350 C in an inert atmosphere of nitrogen and held for two hours at that temperature in order to volitalize as many of the non polymerizable species as possible without changing the

microstructure of the pitch. The cooled pitch is then finely ground for later use in the impregnation stage.

Impregnation of the axial specimens takes place in an inert atmosphere at a temperature of 250 C. The tied fiber bundles are submerged stress-free in a bath of molten pitch where full wetting of the fibers by the pitch occurs. Since oxidation of the graphite fibers inhibits complete wetting, nitrogen is used as the atmosphere. As the fiber is pulled from the pitch bath, it is lightly stretched to extrude the excess pitch from between the filaments. It has been found that pockets of pitch between the filaments can cause stress concentrations that can lead to premature failure when the fully processed specimens are loaded.

The calcination process is the longest of all the specimen preparation procedures. During this stage, the impregnated fiber bundle is loaded into a furnace capable of attaining a temperature of 1000 C. The calcination fixture and furnace is shown schematically in figures 9, and 10. The specimen has a small axial load on it in order to keep the specimen straight and to extrude any excess pitch out of the bundle. The specimen is heated from room temperature to 300 C at a rate of 100 C per hour. At 300 C, the heating rate is reduced to 15 C per hour until a maximum temperature of between 900 C and 1000

C is reached. The extremely slow heating rate through the mesophase transition and crystallization temperature is needed because of percolation caused by reaction products which eventually volatilize and try to make their way to the surface of the mesophase pitch. This percolation, if allowed to occur causes an extremely porous matrix. This stage is the critical one where flaws may develop in the matrix or fiber-matrix interface, which inhibit the full alignment of the matrix basal planes with the fiber axis. The temperature, heating, and cooling rates are automatically controlled by a Honywell-Brown Electronix temperature controller. The controller, furnace, etc. are shown in figure 11.

Graphitization of the fiber bundle is done in an Astra high temperature furnace using argon as the inert atmosphere. The furnace is fully described in a subsequent section. The fibers are hung vertically with a small axial load to prevent warpage. The temperature is increased from room temperature to a maximum temperature of 1800 C where it is held while the basal planes in the matrix align themselves axially with the fibers.

Once graghitization is complete, the specimens are ready for either the tensile rupture tests, or creep testing.

4.2 PREPARATION OF PULL-OUT SPECIMENS

These specimens are cut directly from the Navy billet and are shown schematically in figure 12. Specimens using both the radial fibers and axial fibers are machined with pull-out lengths between 0.25in. and 0.50in. These gage lengths are used to find the shear stress necessary for both the initial break-free of the fibers as well as the friction stress needed to pull the fiber out of the block.

5. HIGH TEMPERATURE MECHANICAL TESTING

5.1 HIGH TEMPERATURE FURNACE

The furnace used for all the mechanical testing as well as the graphitization of the axial test specimens is an ASTRA model 1000T, water-cooled, graphite-resistance furnace, capable of a maximum temperature of 2760 C (5000 F), in an inert atmosphere at a maximum pressure of 20 psig. Automatic temperature control is provided by the use of a silicon controlled rectifier (SCR), combined with either a Boron-Graphite thermocouple, (BGT), for temperatures below 2000 C) or a radiation pyrometer, used for temperatures in excess of 2000 C. A summary of furnace specifications is given below:

MAXIMUM SUSTAINED TEMPERATURE	2760 C (5000 F)
HEATING RATE	Room temperature to maximum temp, 30 min.
HOT ZONE	Cylindrical, 8.0 in. long, 3.0 in. dia.
HEATING ELEMENT	Graphite
THERMAL INSULATION	Carbon felt and powder
ACCESS TO HOT ZONE	Axially from both ends
COOLING	Water cooled, 1.5 gal. per min.
POWER SUPPLY	18 KVA stepdown transformer for 208/230 volt, 60 amp source,

5.2 LOADING SYSTEM FOR PULL-OUT SPECIMENS

The loading frame for this project was designed and built specially for this furnace and is shown in figure 13. The frame consists of a 17 RPM Bodine reversible gear head motor which through a worm, pinion, and bevel gear will turn a 1/2 in. threaded shaft. The non-rotating collar on top of the shaft will displace 0.010 in. per minute by the rotation of the threaded shaft. A hollow rectangular steel brace is placed between the displacement frame and the furnace to stiffen the system. The system is good for loads up to about 150 pounds. The high temperatures inside the furnace required the use of a series of graphite blocks to withstand the loads necessary to test the shear specimens. This chain of loading blocks is shown in figure 14.

5.3 LOADING SYSTEM FOR AXIAL AND CREEP SPECIMEN

The axial specimens for the tensile rupture experiment used the loading frame described above for its higher load capabilities. The creep specimens, however, used an entirely different loading system. Because of the

relatively low load needed for the creep study and the fact that the load must be constant regardless of the axial displacement, a dead weight system was developed. When running a creep test, both temperature and load must be varied, therefore, a shockless loading system using water is used, figure 15. The load path inside the furnace, shown in figure 16, consists of the specimen attached to the top of the furnace with the test section in the middle of the hot zone. Two other sets of fibers are used as an intermediate load bearing system because of their light weight and high strength. These fibers have a cross sectional area five times that of the test section of the specimen. Since creep strain is an inverse power function of the cross sectional area, the creep of the load bearing fibers in all but the test section of the specimen is negligible.

5.4 INSTRUMENTATION

For both loading systems, the force is measured by strain gages attached to a thin piece of aluminum hanging below an aluminum frame work housing the Linear Variable Differential Transformer,(LVDT), for displacement measurement, figure 17. The strain gages, type EA-060-062AP-120 are supplied by Micro-Measurements. The

gages are connected in a four-arm Wheatstone bridge circuit and are excited by a 440 Hz. oscillator built into a HP-7702A two channel strip chart recorder. The system is calibrated for the load range desired and recordings made for each test. The linear variable differential transformer, (LVDT), model 200 DCD, is supplied by Schavitz engineering and has a sensitivity of 50.6 volts per in. The power supply for the LVDT is a dual 15 volt DC regulated power supply. Data is taken off a digital volt meter for recording purposes. Figure 18 is a block diagram showing all the instrumentation and control equipment for the furnace and loading systems.

5.5 PULL-OUT

The pull-out tests were done in two ways. The first used a controlled test length of 0.300 in. for both axial and radial specimens. The reason for this is to provide a direct comparison of average break-free and friction forces required to pull out the respective fibers. The second used axial specimens only and each with a different gage length. The reasoning behind this last series of tests is as follows; The parameters being measured are 1) The force needed to break free the bundle, and 2) the gage length and bundle dimensions in the test section. These

quantities can only be used to find the average stress needed to break-free the bundle, or the maximum force that the bundle will experience. From the shear-lag analysis, appendix B, it is known that the shear stress is a hyperbolic function with respect to length. The general solution for this problem is given as equation 12 in appendix B:

$$F = E_f \pi r^2 \varepsilon_m + C_1 \sinh(\alpha x) + C_2 \cosh(\alpha x)$$

For the specific application to this testing, figure 19 is used in conjunction with the following boundary conditions:

at $X = 0$, $F = 0$

at $X = \ell$, $F = F_{max}$

$v = 0$, $\varepsilon_m = 0$

Where; F = force on the fiber at position X.

F_{max} = force on the fiber outside the matrix.

Note: The term ε_m is defined as the strain of the matrix. The only matrix strain occurring in this model is that due to temperature. Since this analysis is based solely on experimental data, the correction for strain

due to temperature can be associated with the variable b which is defined as the effective radial distance from the fiber into the matrix where the the matrix stress is constant, and beyond which, the shear stress is zero.

From appendix B

$$\alpha = \left[\frac{2G_m}{brE_f}\right]^{\frac{1}{2}}$$

The above boundary equations will give the values for the constants C_1 and C_2 as follows:

$$C_1 = \frac{F_{max}}{\sinh(\alpha \ell)}$$

$$C_2 = 0$$

The force on the fiber then becomes:

$$F = \frac{F_{max}}{\sinh(\alpha \ell)} \sinh(\alpha x)$$

Recalling that

$$\tau = \frac{1}{2\pi r} \frac{dF}{dx}$$

$$\frac{dF}{dx} = \frac{\alpha F_{max} \cosh(\alpha x)}{\sinh(\alpha \ell)}$$

Therefore: At $x = \ell$

$$\tau_{max} = \frac{\alpha F_{max}}{2\pi r \tanh(\alpha \ell)}$$

Dividing both sides by

$$\tau_{ave} = \frac{F_{max}}{2\pi r \ell}$$

Gives

$$\frac{\tau_{max}}{\tau_{ave}} = \frac{\alpha \ell}{\tanh(\alpha \ell)}$$

Where;

τ_{ave} is measured, known

ℓ is the gage length, known

α is an unknown variable

τ_{max} is an unknown variable

This leaves two unknowns, τ_{max}, and α, and only one equation. Since it is only necessary to find the value for τ_{max} and α, at only one point, and that these should be material constants that vary only with temperature, an iteration process can be employed to solve for the unknowns. This process must employ several data points for each temperature in order to get a fair representation of the data. This process is shown in detail with the following example of four axial pull-out specimens tested at a temperature of 1000 C.

Specimen	Temp (C)	Gage length (in)	τ ave (psi)
A-9	1000	0.225	1313
A-12	1000	0.303	1030
A-15	1000	0.310	1257
A-18	1000	0.300	1029

By assuming that τmax is the same for all specimens at this temperature, curves can be plotted for τmax vs. α. This procedure is followed for each of the data points finding the values for α where the curves cross each other. The average value for α is then plugged back into the equations for τmax for each point. This iteration process is continued for each temperature with the results of τmax for each of the axial pull-out specimens listed in table 3 with both the average value and standard deviation for the three temperatures examined.

5.6 CREEP

Analysis by Quan and Sines, in appendix A, has shown that upon heating, there is a tensile stress in the radial direction and that this stress is greater than that in the circumferential direction. In order to reduce the stress

in the radial direction, it may be advantages to promote creep. In order to model this form of stress relief, we assume that a perfect bond exists between the radial and circumferential fiber bundles. With these boundary conditions, the classic model of stress relaxation of a rod, fixed at both ends and heated, may be used.(ref 2)

In the following model, developed by Quan and Sines (ref 2) it is assumed that the only appreciable creep strain is in the radial yarn. The assumed unit cell has 25% radial fiber and the remaining 75% has properties along the radial direction similar to that of the matrix. If a balance of force exist between the matrix and fiber, ie. perfect bonding, then the following relation between the tensile stress in the fiber and the compressive stress of the matrix applies:

$$\sigma_m = \frac{1}{3}\sigma_f$$

Since the stress term in the creep equation behaves in a power law fashion, this makes the matrix in the radial direction relatively insensitive to creep.

The general creep equation used in this model is:

$$\frac{d\epsilon}{dt} = A\sigma^n \exp \frac{-\Delta H}{RT}$$

Where $\epsilon \equiv$ creep strain.

Consistent with this model is the expression for the stress at any time t, for a given temperature T.

$$\sigma = \left[(1-n)AEt \exp \frac{-\Delta H}{RT} + (E\sigma_e)^{1-n}\right]^{\frac{1}{1-n}}$$

Using the above equation, the values A, n, E, and H can be found by experiment.

6 RESULTS AND DISCUSSION

6.1 PULL-OUT

A direct comparison was done between pull-out specimens having either the radial or the axial fibers as the test fibers. Three each of the two types of specimens were tested at each of three different temperatures. Each specimen had a gage length of $0.300 \pm .015$. The results of this comparison are shown in figure 21 and table 4. Notice that the averages of the break-free shear stress for the axial fiber bundles had a significantly higher value at the 1500 C temperature, as well as a much lower variation of stress than the radial fiber bundles. This supports the belief that the interfacial cracking of the bundle-matrix interface of the radial fiber bundles shown in figure 1, can significantly reduce the shear load capability of the radial fiber bundles. A little surprising is the fact that at 1000 C, the same significant difference in the break-free shear stress was not seen. One possible explanation for this is that cracks do exist between the fiber and the matrix of the axial fiber, however, the magnitude of the size of these cracks is considerably less than the radial cracking, and that at a high temperature, thermal expansion of the

matrix closes the axial cracks first creating a large normal force jamming the fiber in place. Also included in this comparison is the friction load carried by the fiber bundles after they have broken free from the matrix. Again as expected the axial fiber bundles show a higher frictional shear stress capability than the radial fiber bundles. This can be explained by the thermal expansion of the matrix first having to close the wider cracks in the interface between the radial fiber bundles and the matrix before a normal force can be applied to the fiber bundle. In some instances the data from the pull-out tests showed that the radial fiber bundle had completely broken free from the matrix and was held in by the friction force only. This is shown by figure 22, which shows the data from three representative tests as graphed by a force vs. time plot taken during the test.

A second series of pull-out tests were performed using the axial specimens only. This test included pulling out bundles from the test specimens with different gage lengths. Using this data and the equations developed in the previous section, the average peak shear stress can be found for each temperature. Since the axial specimens showed no visible signs of bundle-matrix cracking, even with the fluorescent dye at 10X magnification, it was concluded that this data can be used to establish the

interfacial shear strength of the bundle-matrix interface. The results of this data can then be used to predict the failure of a composite during processing. The results of this test is shown in figure 23. Notice the increase in strength with temperature for the average and calculated peak shear stress. This is consistent with the general knowledge that the strength and stiffness of carbon increases in magnitude with temperature until about 2000 C before falling off. There is a question of whether cracks in the axial direction exist or not. There are no visible cracks and the above analysis assumed that cracks do not exist, however, data from break-free experiments at 1000 C did not show the expected increase in strength of the axial specimens over the radial specimens and, the data from specimen A-13, figure 22A, show that there was no clear break free point, only a friction force that held the fiber in the matrix.

6.2 AXIAL CREEP AND RUPTURE

Graphitization of the axial test specimens made in-house presented a problem. The furnace atmospheric seals melted before the furnace reached the desired graphitization temperature of 2500 C, in fact, the maximum temperature that the furnace could be safely run was 1800

C. The remaining axial specimens made in-house, those that were not oxidized when the seals melted, were heat treated at 1800 C. Figure 24 shows a photomicrograph of the test section of an axial fiber made in-house, notice the smooth surface which shows that very little percolation occurred during processing. When tested in creep at 1800 C the specimen showed no elongation with an axial stress of 11.4 ksi for 20 min. This was not surprising since Ouan and Feldman found no appreciable creep with the same specimens before reaching a temperature of 2200 C.(ref 7)

The in-house axial specimens were also tested to rupture at room temperature. these specimens included some graphitized as well as some calcined and simply impregnated. The manufacturers data for HM-3000 shows a dry ultimate strength of 350 ksi for the fiber bundles. The nine specimens tested all broke in the test areas at values between 185 and 260 ksi. One possible explanation for this is that there may be matrix pockets between the filaments creating stress concentrations. The data showed that there was little difference in the strength of the fiber bundles tested at different stages of in-house processing.

7 CONCLUSION

The findings of the original crack study by Sines and Cohen (ref 1), suggested that the level of stress in the radial fiber bundle may have something to do with the circumferential crack pattern observed. The assumption that the radial fiber is the most severely stressed fiber is confirmed by simple analysis by both Quan and by Jortner in appendix A (ref 2). The usefulness of the radial fiber bundle in reducing the circumferential composite stress is dependent on them being strong and well-bonded to the surrounding matrix. If the fiber bundle debonds during processing, its effectiveness in relieving the hoop stress is minimal and would be economically unfounded to have radial bundles, if this is their only function. In this study it was shown that the radial fiber had indeed at least partially debonded from the surrounding matrix. The analysis by Cohen and Sines shows that the radial bundle shear stress is greater at both the inner and outer radius than in the center. An exact analysis and prediction of when the fiber may pull free is beyond the scope of this report. The need for accurate creep data is essential in finding a way to relieve the stress in the radial bundle to a level below the strength of the bundle-matrix interface, this would

enable the radial fiber to have a better chance of doing some good in reducing the stress in the circumferential direction.

ACKNOWLEDGMENTS

Sincere appreciation is extended to Steve Lau and Paul Lewis for their help in the preparation of test specimens.

REFERENCES

(1) B. Cohen, G. Sines, "Fabrication Stress and Crack Morphology of the Three Dimensional Cylindrically Woven Carbon - Carbon Composites", UCLA-ENG-81-26, University of California Los Angeles, September 1981, 164 Pages.

(2) Douglas Quan and George Sines, "The Effects of Radial Yarns - Three Dimensionally Reinforced Carbon - Carbon Composites", UCLA-ENG-84-22, University of California, Los Angeles, July 1984.

(3) D. Hull, "Introduction to Composite Materials", Cambridge University Press 1981.

(4) Evangelides, Chang, Gyetvay, "Fiber-Matrix Thermal and Mechanical Properties", ONR Interim Report, The Aerospace Corporation, February 1981.

(5) J.S. Evangelides, G.H. Sines, and S.B. Batdorf "Damage Mechanisms and Modeling of Carbon-Carbon Composites", UCLA-ENG-79-75, University of California Los Angeles, May 1979, 151 Pages.

(6) Walrath, Adams, "Test Methods Developement for 3-D Cylindrical Weave Carbon - Carbon Composite Materials", ONR Interim report, September 1981.

(7) Hashin, Z., et. al., "Evaluation of Material Guidance Codes for Carbon - Carbon Materials", Technical report AFML-TR-77-94, June 1977.

(8) L.A. Feldman, "High Temperature Creep of Carbon Yarns: First Annual Report", ONR Annual Report, F04701-82-C-0083, The Aerospace Corporation, September 1983.

(9) Iannuzzi, F. A., et. al., "Manufacturing, Physical, Mechanical, Thermal, Transport, Electrical and Chemical Properties of Carbon and Graphite Filaments Yarns and Fabrics", Technical Report AFML-TR-78-60, February 1979.

(10) Odom, Adams, "Axial Test Methods Developement for 3-D Cylindrical Weave Carbon - Carbon Composite Materials", ONR, N00014-77-C-503, Interim Technical Report November 1983.

PROPERTY	HM-3000	HM-10000
Density (lb/in^3)	0.067	0.066
Strength impreg. (Ksi)	350	355
E_A (psi)	54×10^6	50×10^6
E_T (psi)	1.5×10^6	3.5×10^6
Diameter (Um)	7.2	7.5
α_A (/°F)	*	1.39×10^{-6}
α_T (/°F)	*	7.5×10^{-6}

Table 1 Conditioned properties of fibers used in this study at room temperature from their manufacturer's data

PROPERTY	COAL TAR PITCH 277CP-15V
Density (gr/cc)	1.35
Cooking Value (%)	48.2
Benzene Insolubles (%)	12 - 18
Quinoline Insolubles (%)	4 - 8
Ash	0.23

Table 2 Properties of 277CP-15V coal tar pitch matrix from their manufacturer's data

TABLE 3A. ALPHA, AVERAGE AND PEAK SHEAR STRESS FOR ROOM TEMPERATURE AXIAL PULL-OUT SPECIMENS

SPECIMEN	TEMPERATURE (C)	τ_{ave} (psi)	ALPHA (1/in)	τ_{max} (psi)
A-5	ROOM	1044	4.5	2081
A-6	ROOM	877	4.5	1433
A-7	ROOM	1085	4.5	1795
A-8	ROOM	690	4.5	1171
A-11	ROOM	1190	4.5	1838
A-13	ROOM	921	4.5	1409
A-14	ROOM	1154	4.5	1798
AVE. (PSI)		994		1646
STANDARD DEVIATION (%)				19.2

TABLE 3B. ALPHA, AVERAGE AND PEAK SHEAR STRESS FOR 1000 C AXIAL PULL-OUT SPECIMENS.

SPECIMEN	TEMPERATURE (C)	τ_{ave} (psi)	ALPHA (1/in)	τ_{max} (psi)
A-9	1000	1313	4.18	1679
A-12	1000	1030	4.18	1536
A-15	1000	1257	4.18	1393
A-18	1000	1094	4.18	1615
AVERAGE (PSI)		1174		1557
STANDARD DEVIATION (%)				7.9

TABLE 3C. ALPHA, AVERAGE AND PEAK SHEAR STRESS FOR 1500 C AXIAL PULL-OUT SPECIMENS

SPECIMEN	TEMPERATURE (C)	τ_{ave} (PSI)	ALPHA (1/in)	τ_{max} (PSI)
A-10	1500	1576	2.8	2006
A-16	1500	1562	2.8	1830
A-17	1500	1620	2.8	1991
AVERAGE (psi)		1586		1940
STANDARD DEVIATION (%)				4.9

Table 3. Values for Alpha, τ_{ave}, and τ_{max} for pull-out specimens using the axial bundles.

SPECIMEN	TEMPERATURE	AVERAGE BREAK FREE SHEAR STRESS PSI	AVERAGE FRICTION SHEAR STRESS PSI
R-14	ROOM	1660	1270
R-15	ROOM	1030	513
R-17	ROOM	*	866
A-11	ROOM	1190	-
A-13	ROOM	*	921
A-14	ROOM	1150	884
R-12	1000	1179	588
R-18	1000	1203	879
R-6	1000	1308	780
A-12	1000	1030	914
A-15	1000	1257	948
A-18	1000	1094	931
R-13	1500	1016	581
R-16	1500	1150	842
R-10	1500	1697	674
A-10	1500	1602	1210
A-16	1500	1560	1260
A-17	1500	1620	1305

* Fiber pulled free without a definite break free point

- When fiber let go, it pulled out completely

Table 4. Data for radial and axial shear specimens with a gage length of approximately 0.300 in.

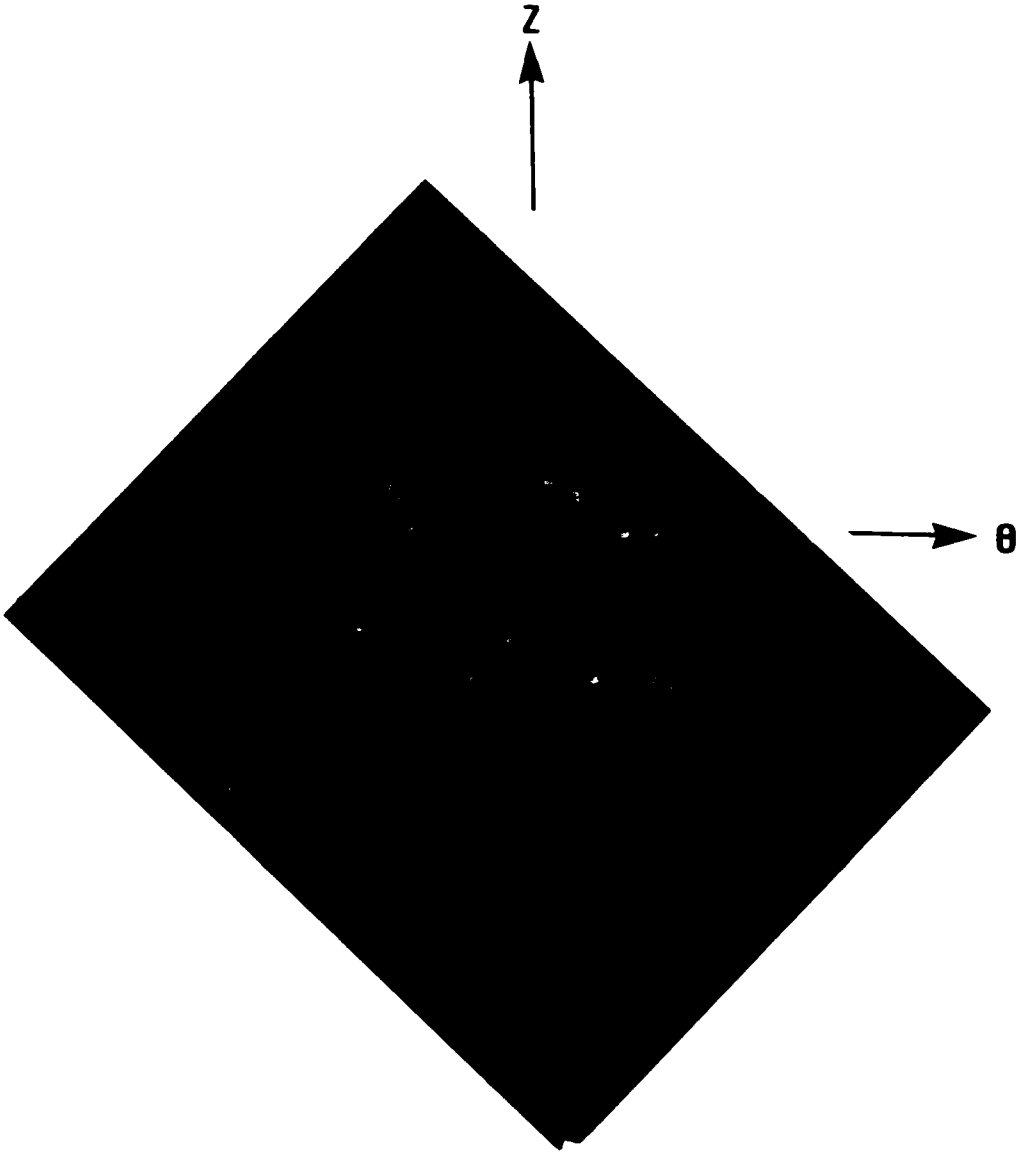

The white lines in the figure are cracks where flourescent dye-penetrant has wicked into them. The small squares and long bands of dark material is the matrix while the smaller lighter rectangles are the fiber bundles. Cracking is apparent inside the bundle as well as in the bundle-matrix interface.

Figure 1. Photomicrograph shows the θ-Z plane of a billet coupon.

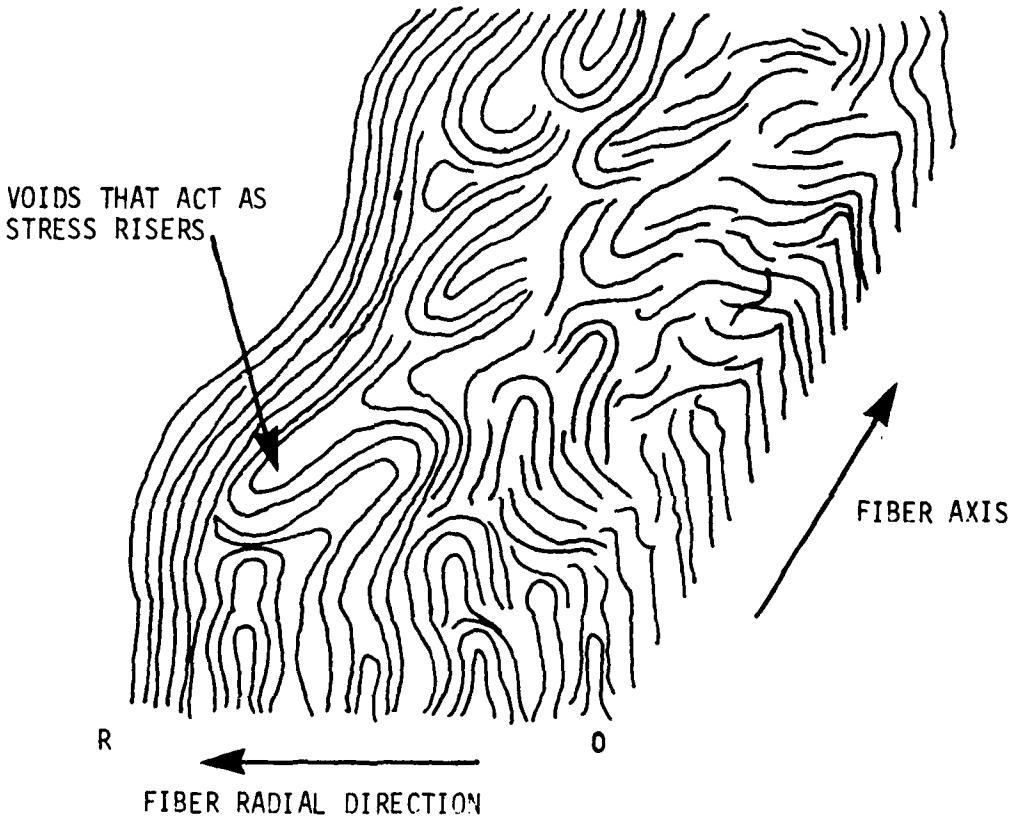

Figure 2. Schematic Representation of basal plane alignment VS. radius for a typical PAN based filiment.

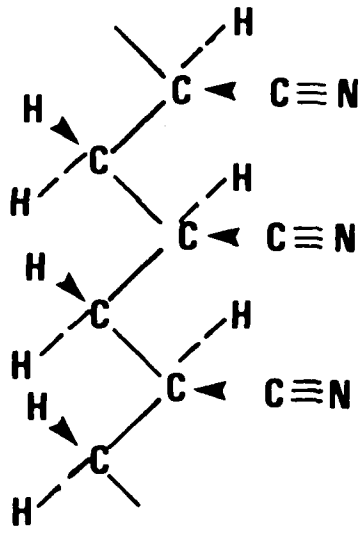

Figure 3. Chemical representation of the chain polymer polyacrylonitril.

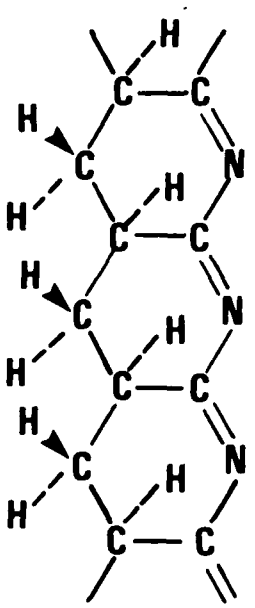

Figure 4. Ladder ploymer created by stretching and heating the PAN polymer, thereby aligning the basal planes.

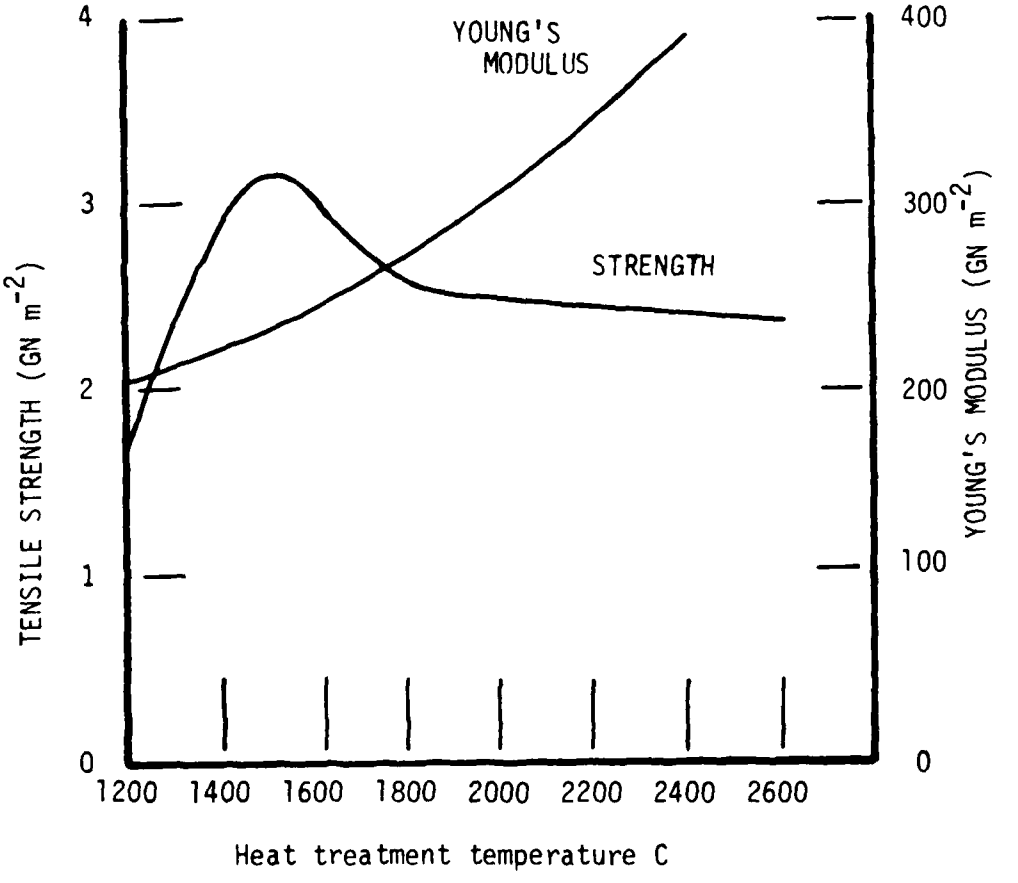

Figure 5. A characteristic plot of strength and modulus VS. graphitizing temperature for both type I, and type II PAN fibers.

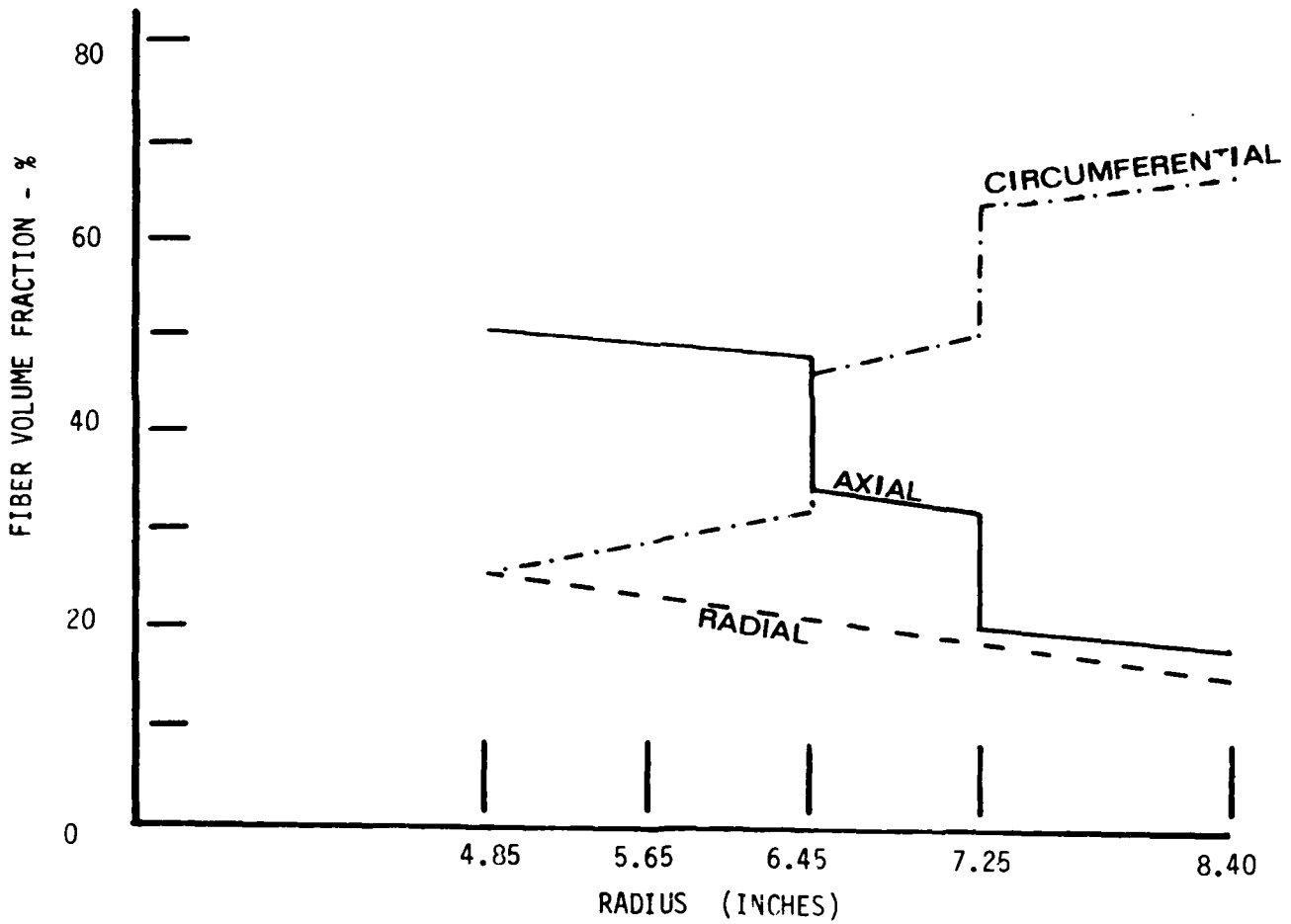

Figure 6. Variation of fiber volume fraction with radius of the billet.

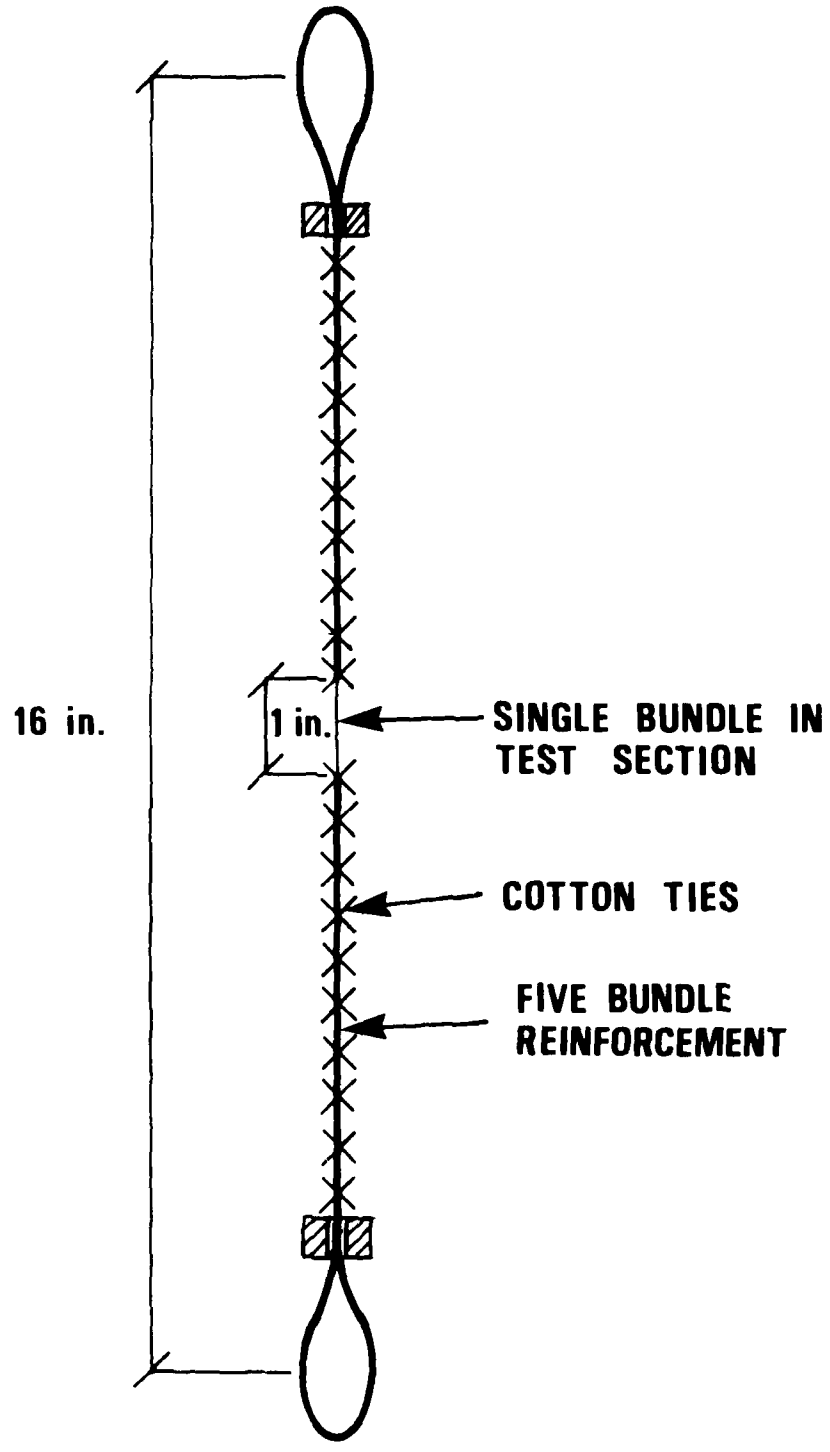

Figure 7. Schematic representation of test specimens used for uniaxial tensile rupture and creep experiments.

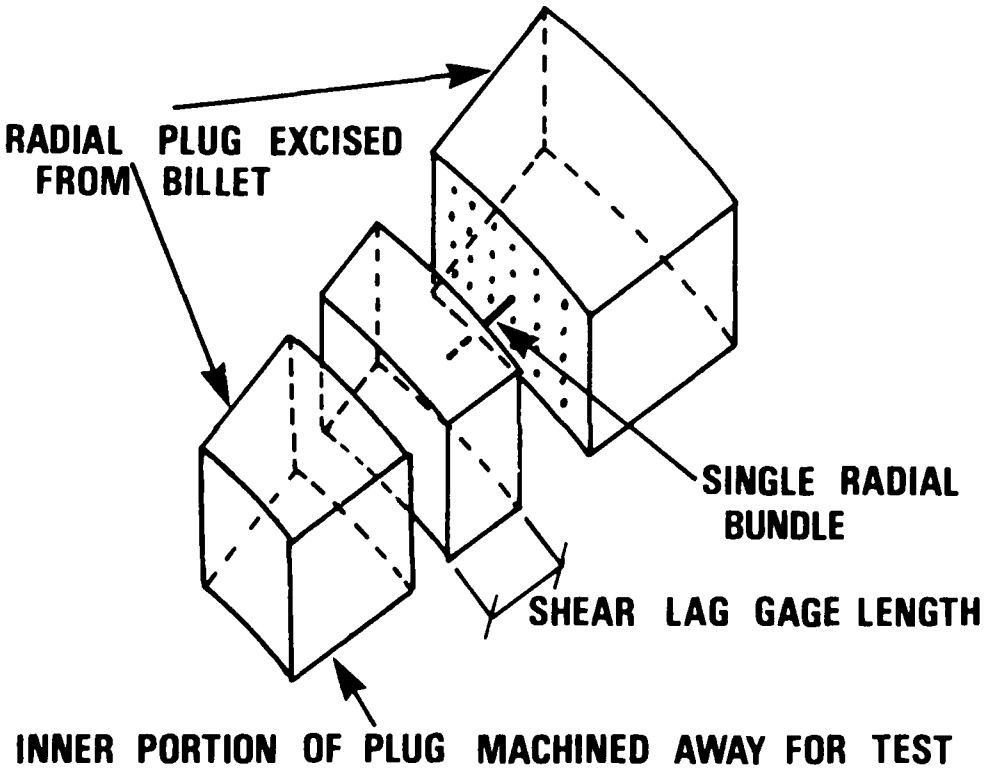

Figure 8. Schematic representation of a radial plug excised from the Navy billet.

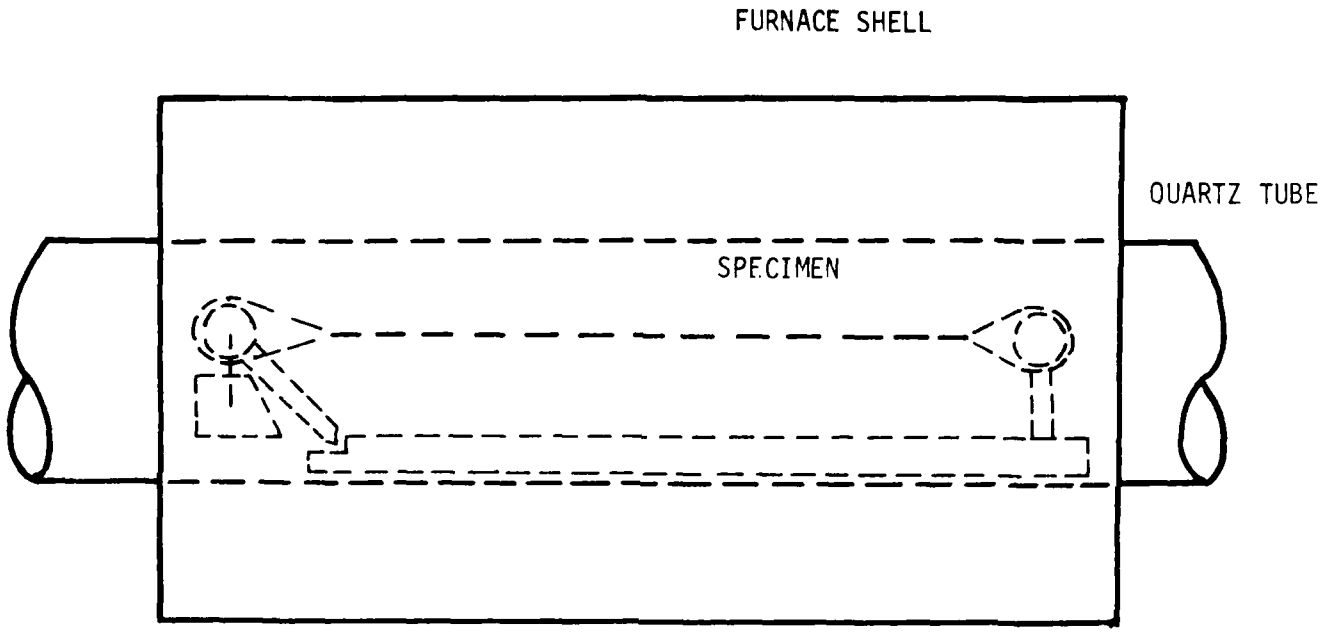

Figure 9. Schematic representation of the calcination fixture inside the tube furnace.

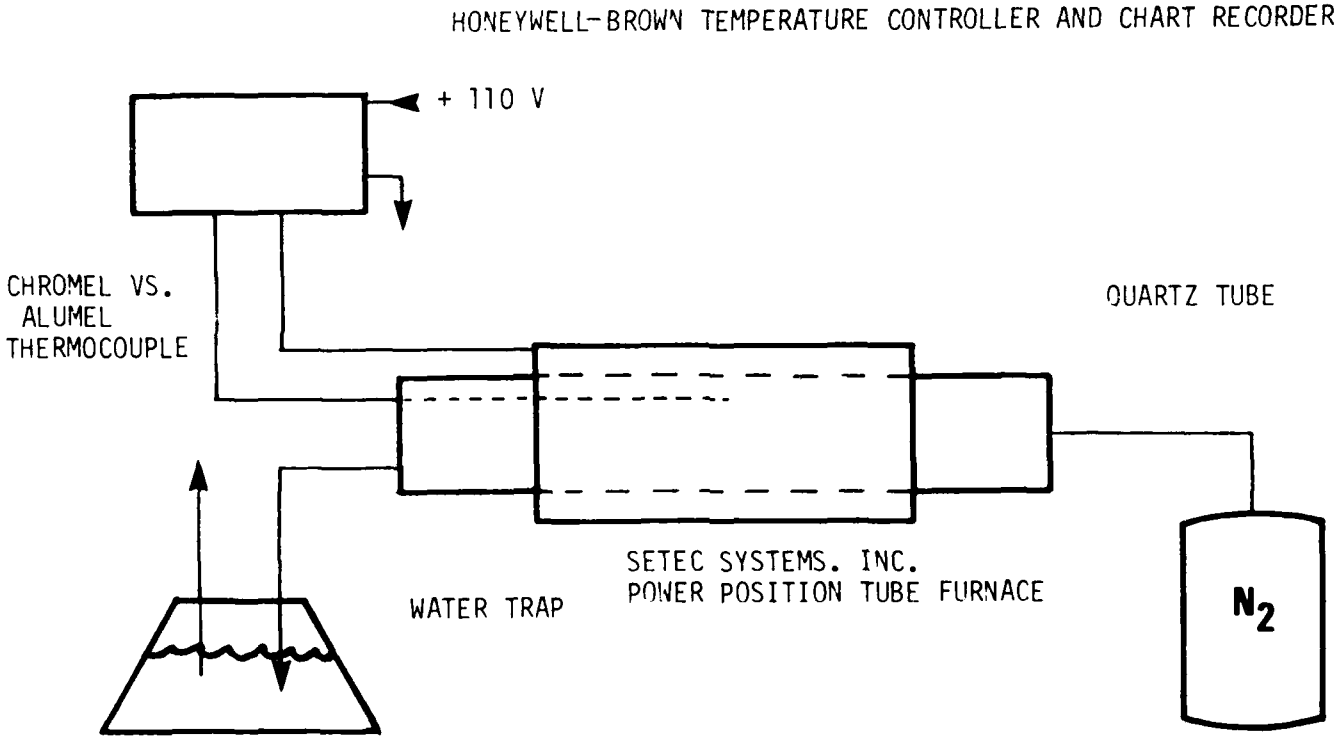

Figure 10. Block diagram of calcination furnace and instrumentation.

Figure 11. Photograph of the calcination furnace and automatic controller/recorder.

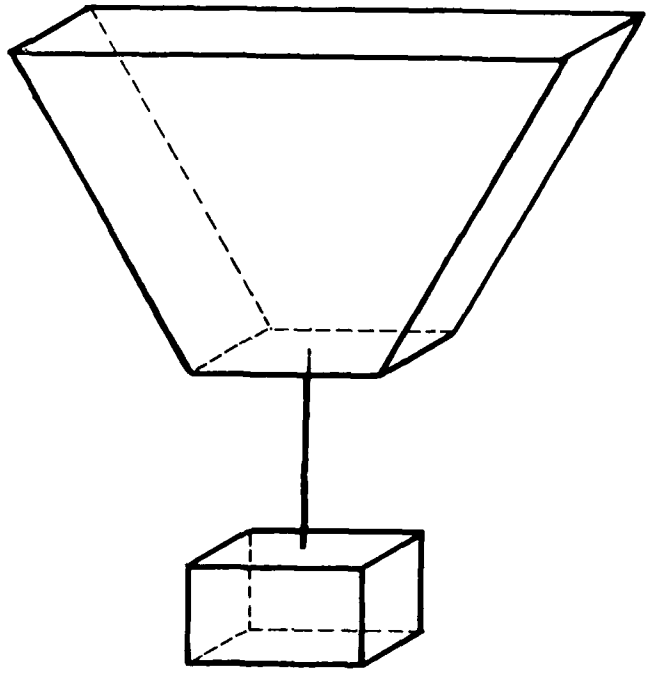

Figure 12. Shear lag specimen for both axial and radial fiber pull-out.

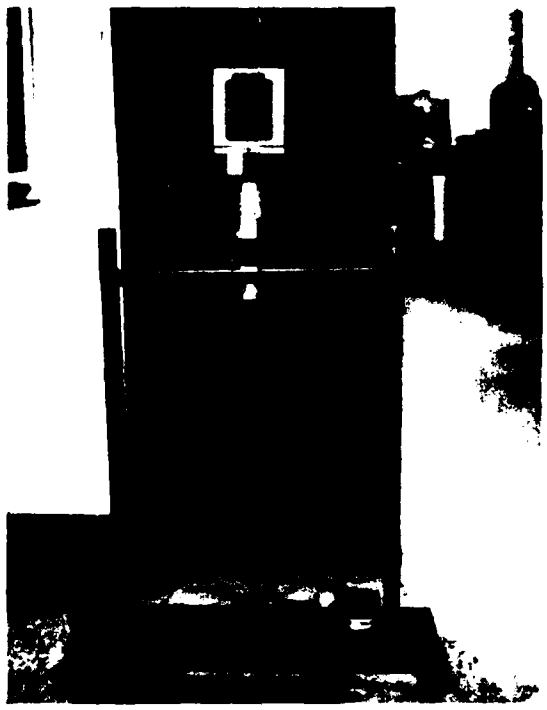

Figure 13. Photograph of displacement frame used to load both the pull-out specimens and axial rupture specimens.

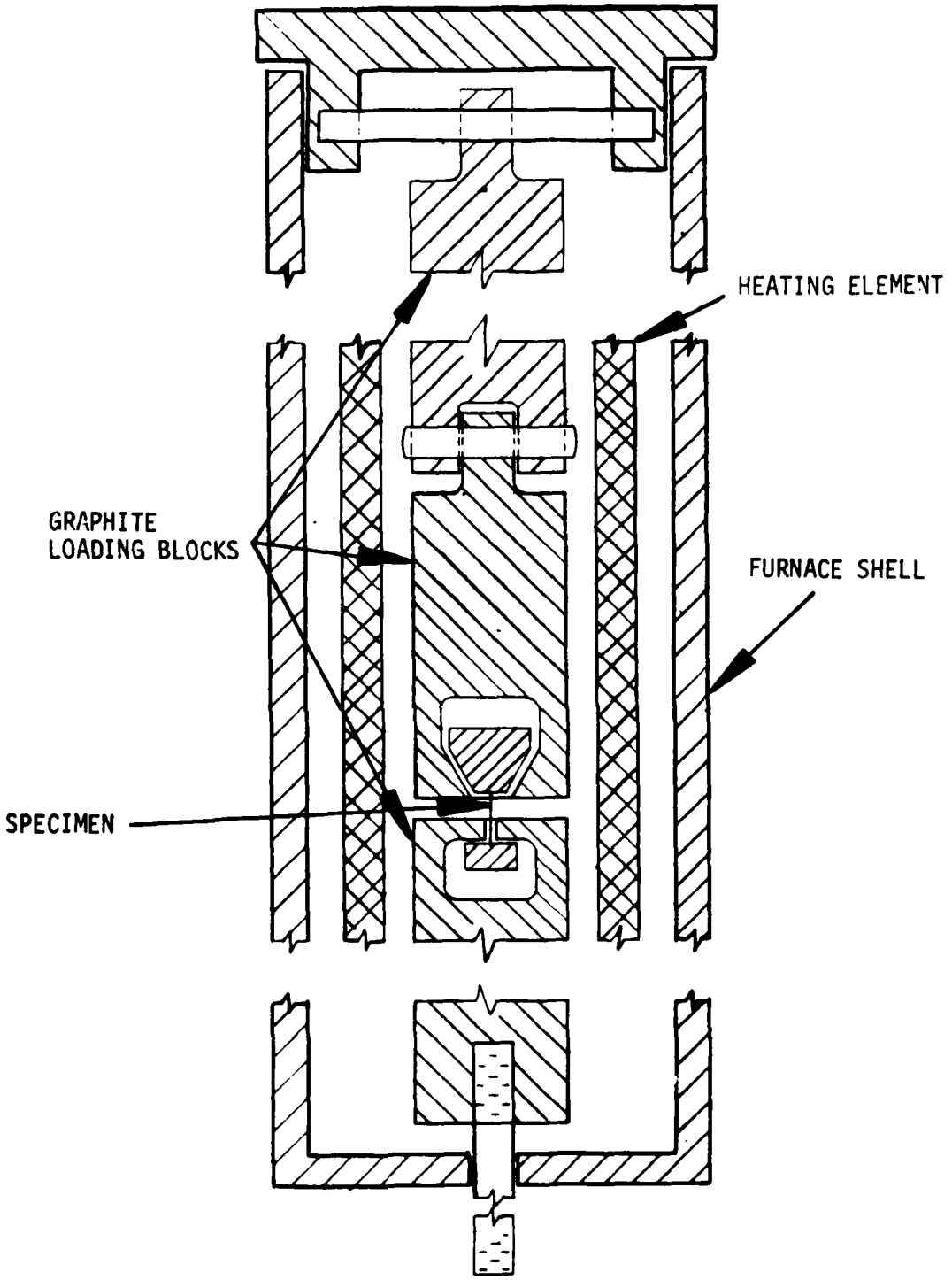

Figure 14. Graphite loading blocks for pull-out specimens

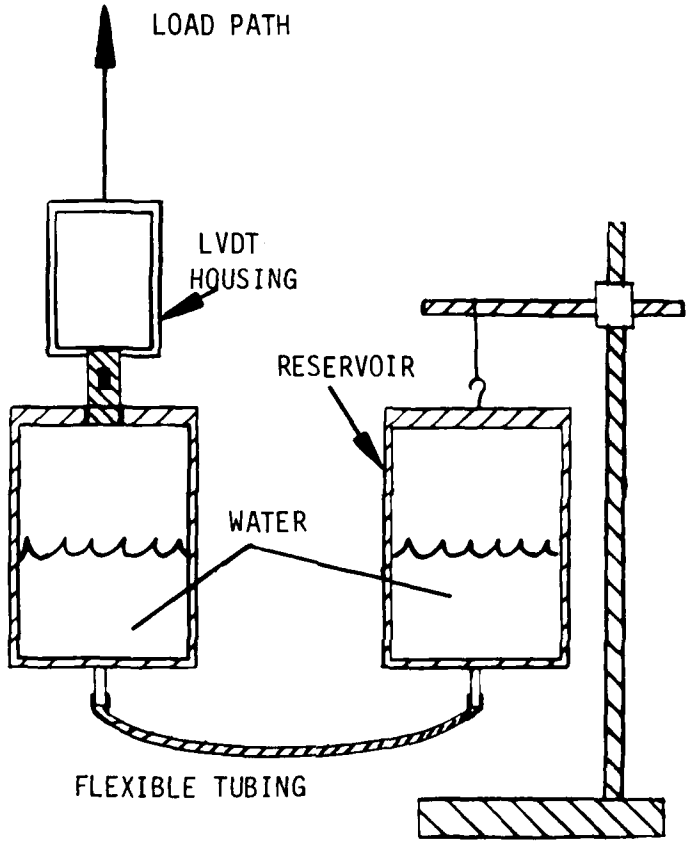

Figure 15. Shockless loading system using water and an adjustable reservoir.

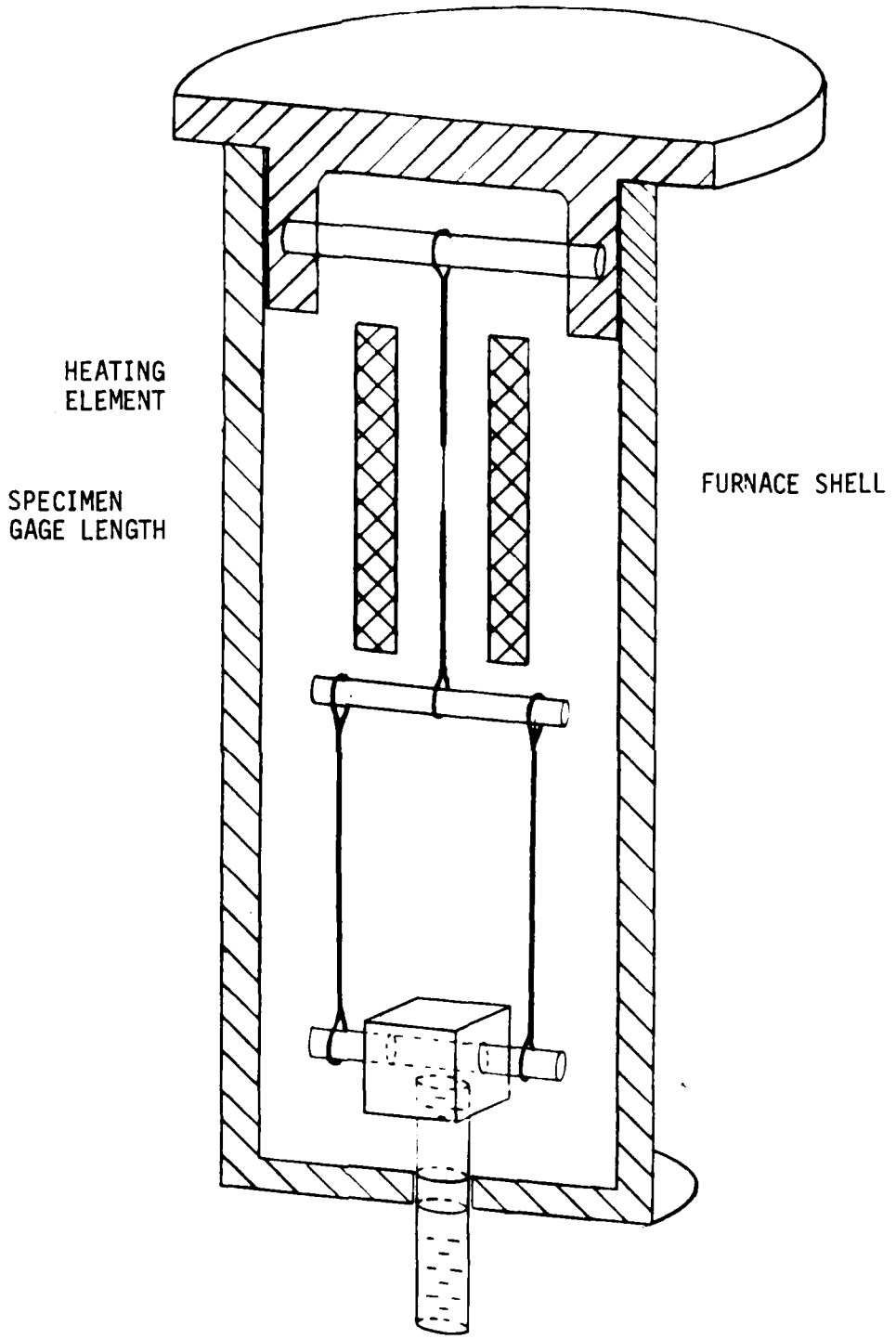

Figure 16. Furnace load path for axial creep and rupture specimens

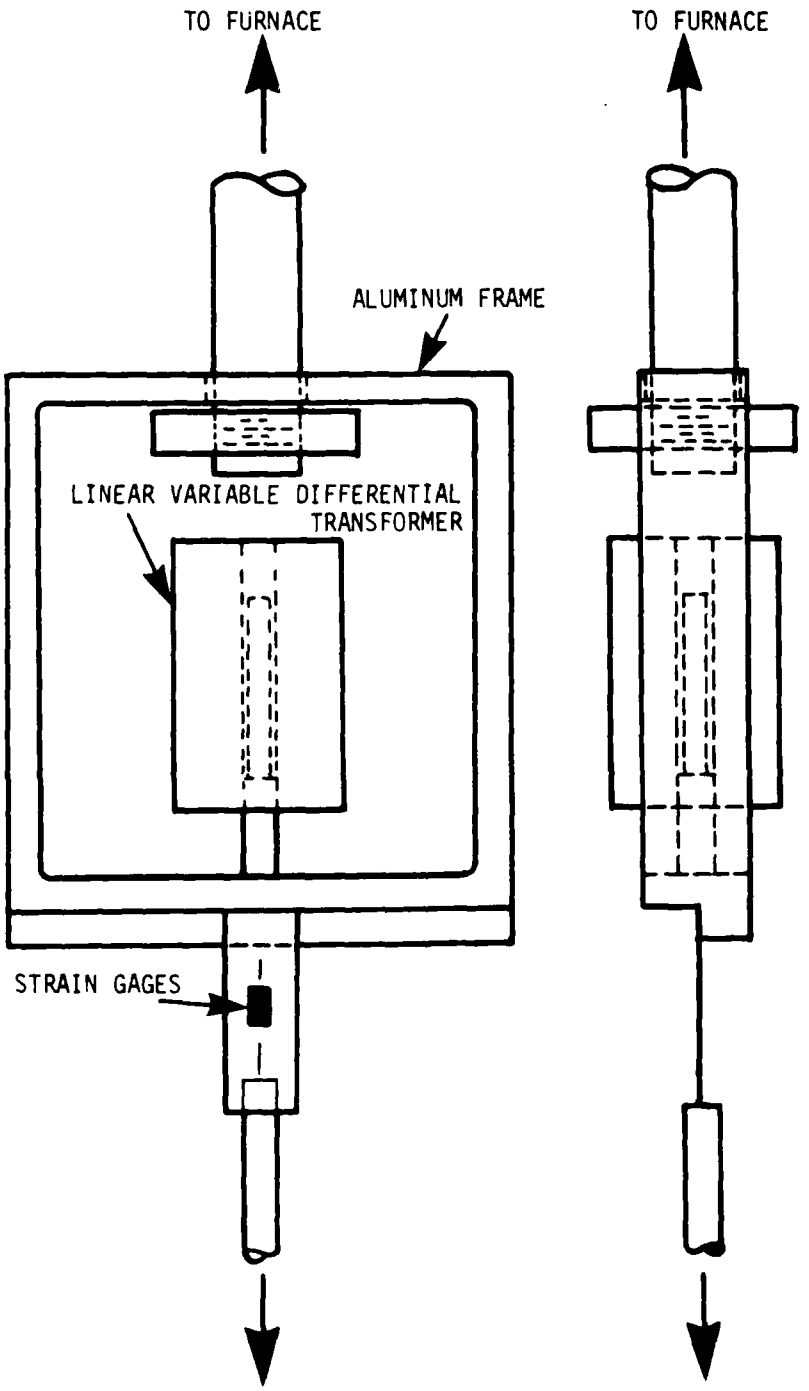

Figure 17. Transducer system for both load and displacement.

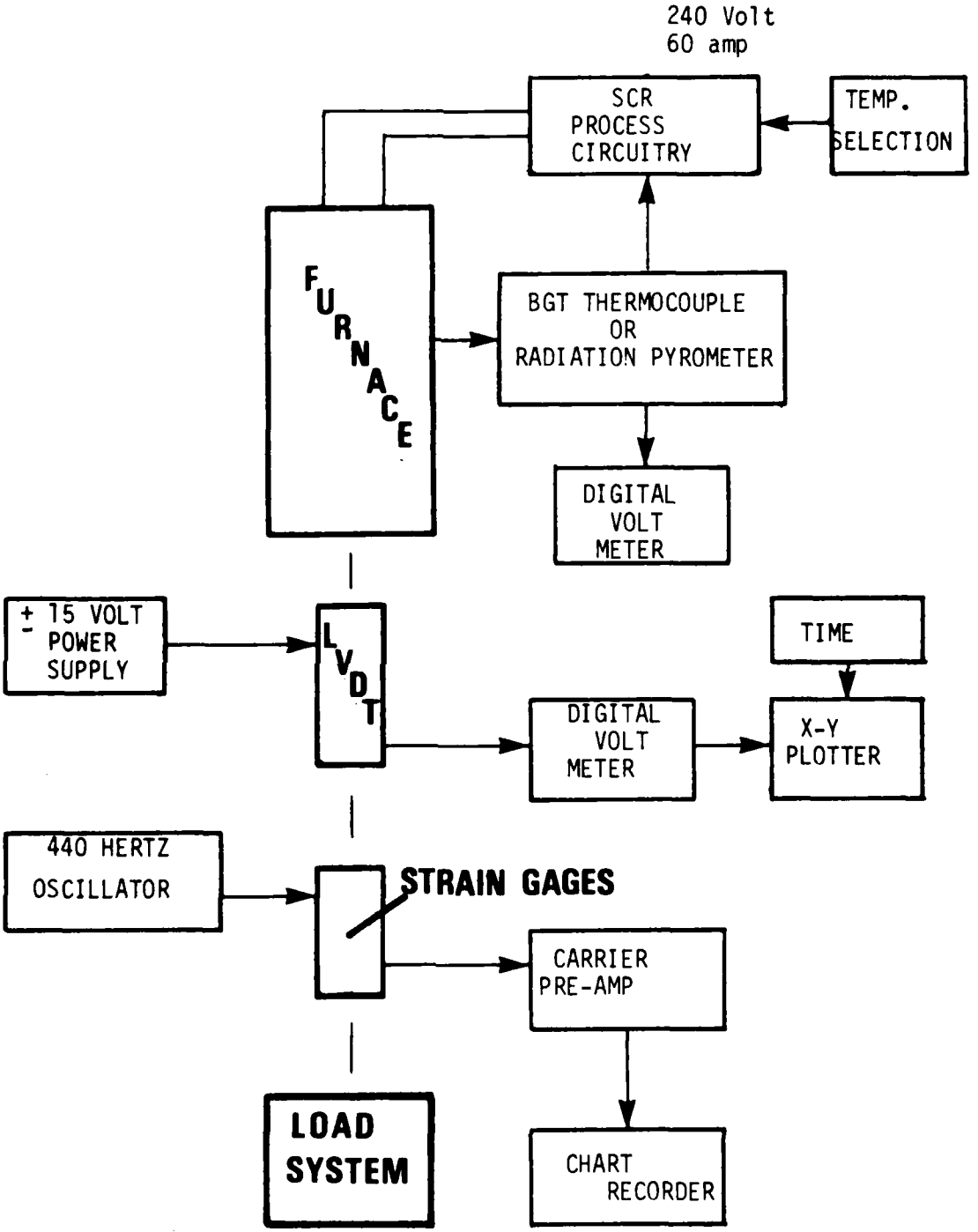

Figure 18. Block diagram of instrumentation and furnace control equipment.

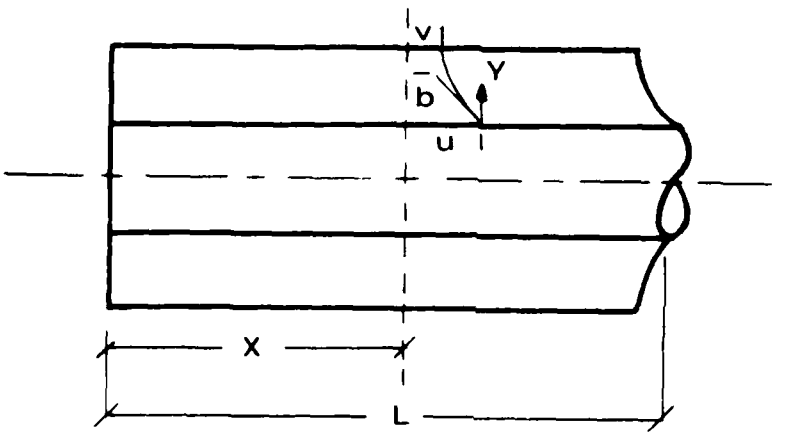

Figure 19. Shear lag theory model for specific application to the fiber pull-out experiments.

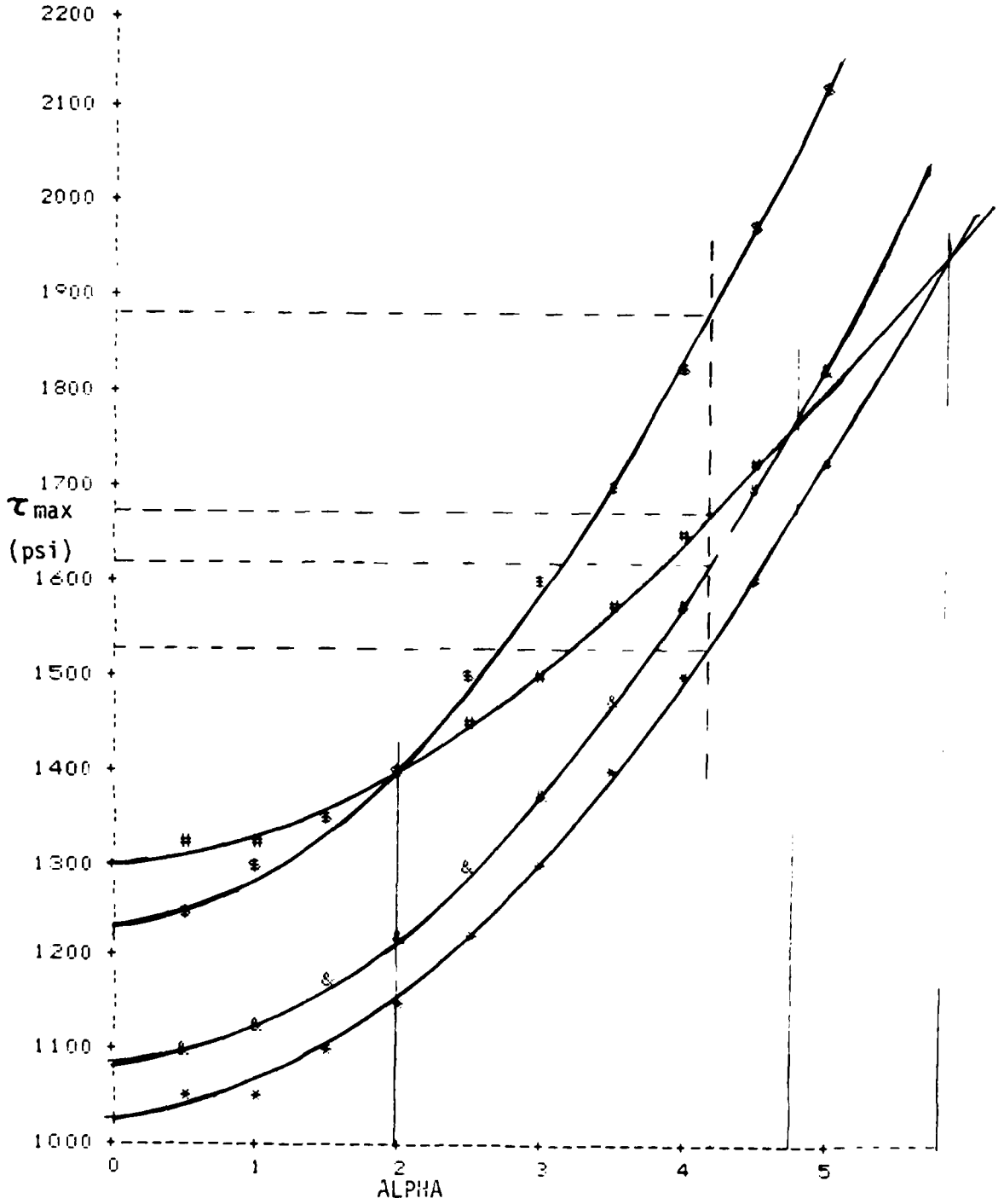

Figure 20. τ_{max} VS. Alpha for pull-out specimens at 1000 C.

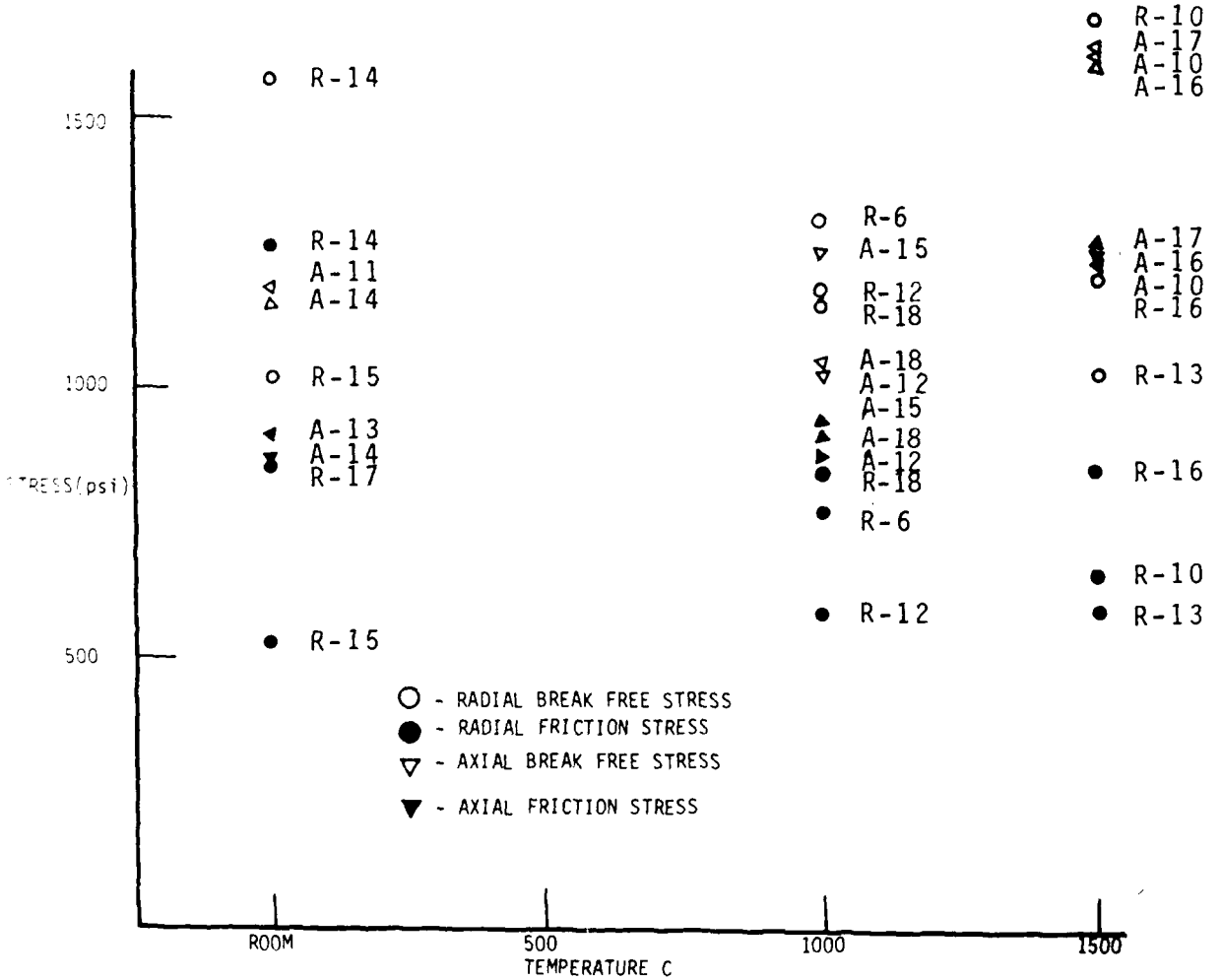

Figure 21. Variation with temperature of the average break-free and friction shear stress for radial pull-out specimens with a 0.300 gage length.

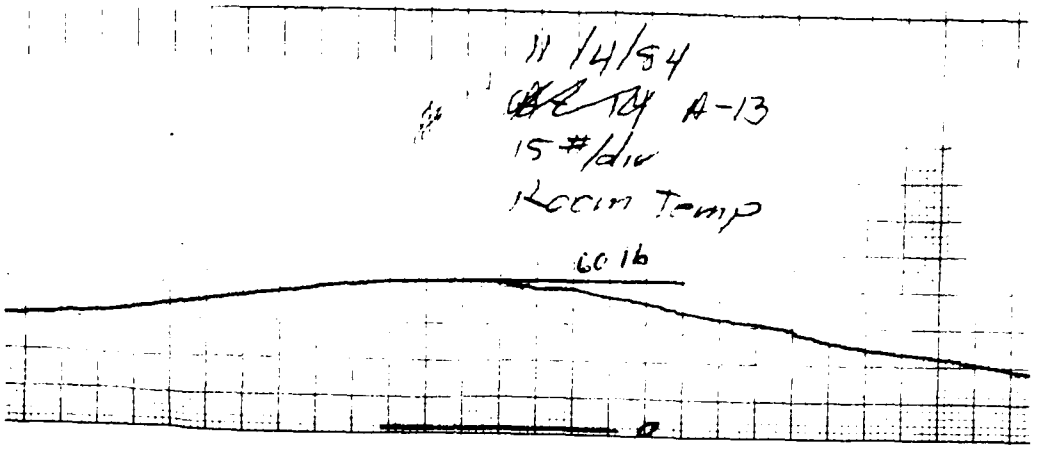

(A) Plot of shear pull-out with no clear break free point, only friction.

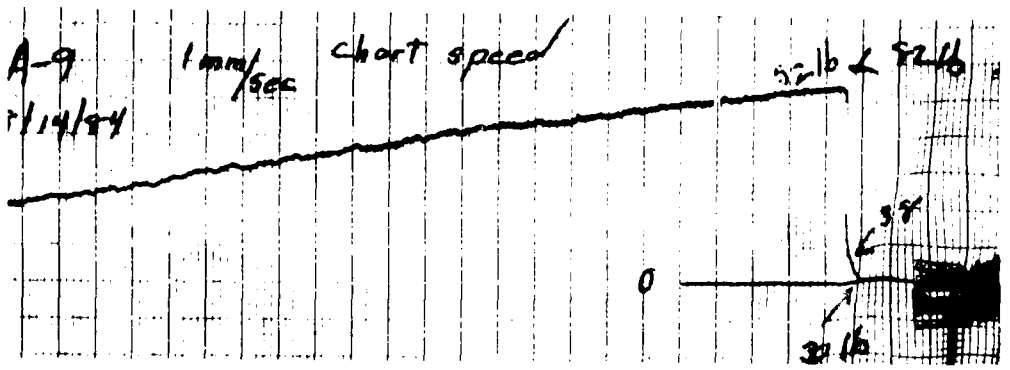

(B) Plot showing complete pull-out of fiber after break free point

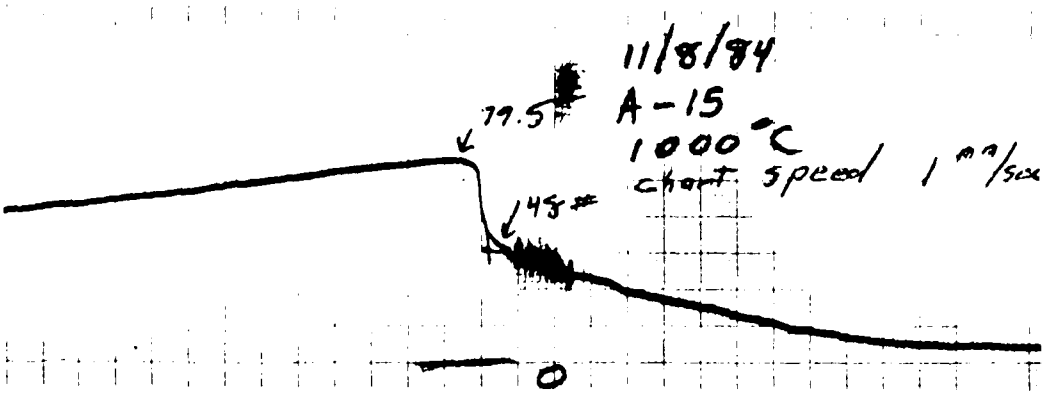

(C) Ideal case showing breakfree point and transition to friction

Figure 22. Data plots of three representative shear pull-out tests.

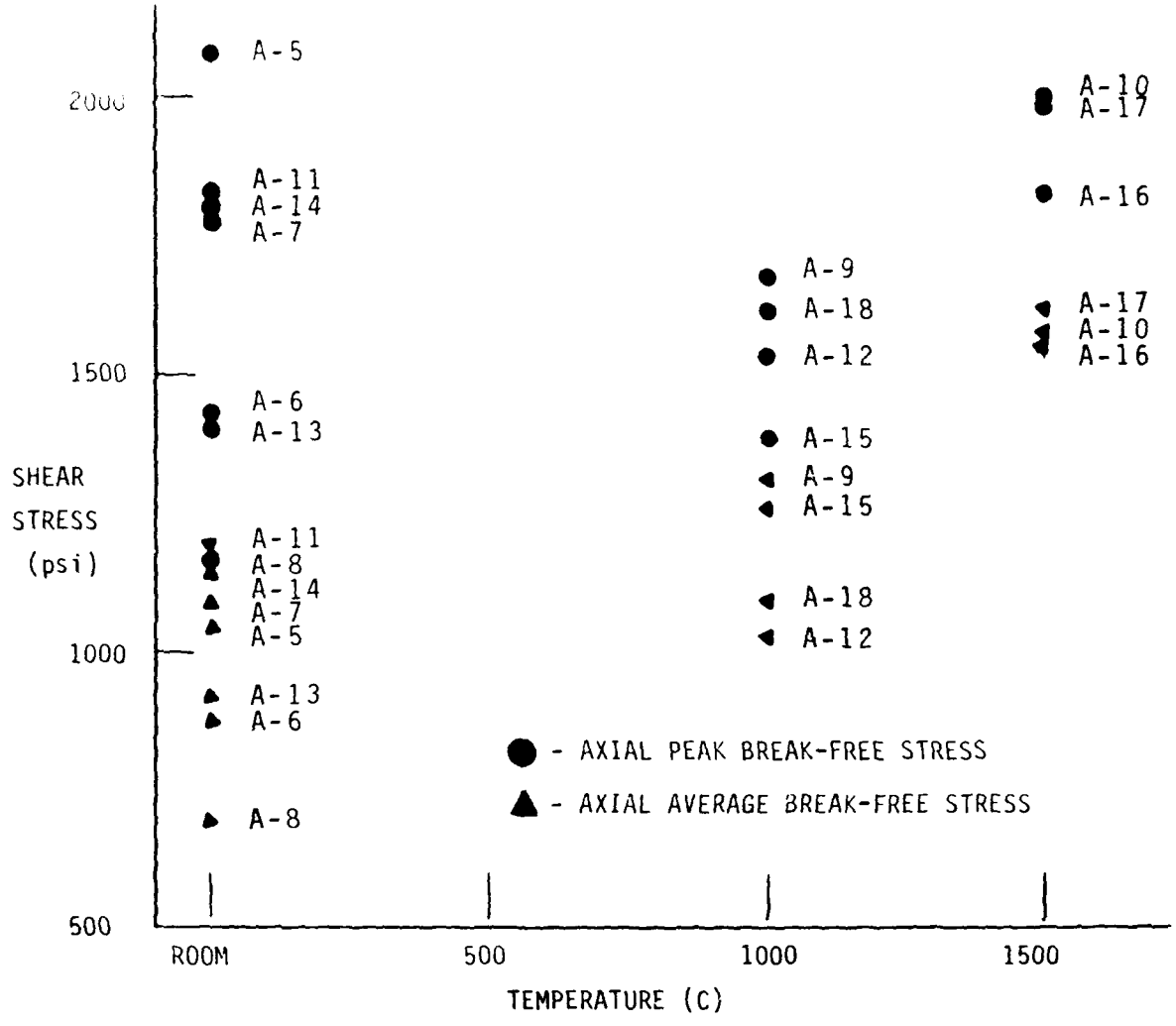

Figure 23. Variation with temperature of the calculated peak bonding shear strength and experimentally determined average shear strength for axial bundle pull-out tests.

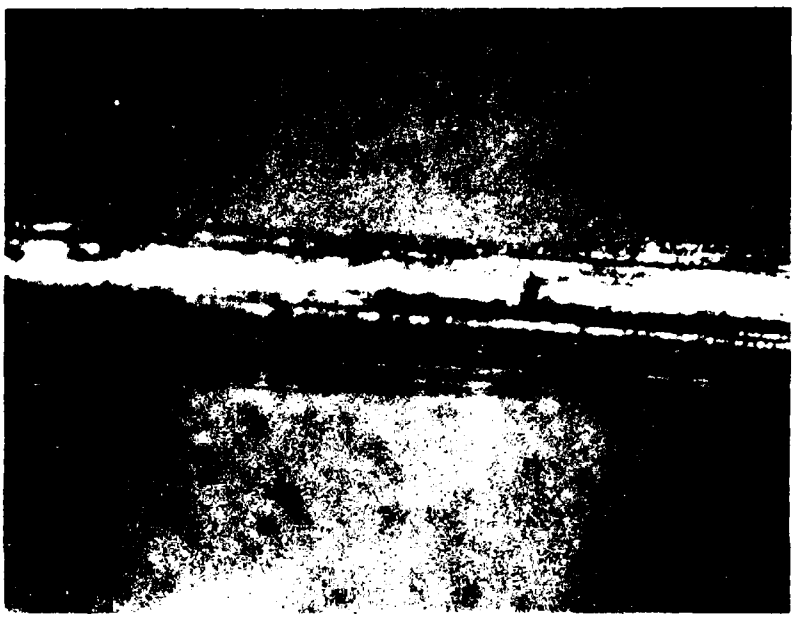

Figure 24. Photomicrograph of creep specimen test section after graphitization at 1800 C. Notice the smooth surface showing very little percolation.

APPENDIX A

THERMALLY INDUCED RADIAL STRESS IN A CYLINDRICAL WEAVE CARBON-CARBON COMPOSITE

The following simple analysis gives a rough estimation of the relative magnitudes of the maximum radial stress to that of the circumferential stress. For the purpose of simplicity, the circumferential stress at the outer and inner radius are taken as equal and opposite.

$$(\sigma_{\theta\theta})_o = -(\sigma_{\theta\theta})_i = | \sigma_{\theta\theta} |$$

This implies:

$$(\varepsilon_{\theta\theta})_o = -(\varepsilon_{\theta\theta})_i = | \varepsilon_{\theta\theta} |$$

From analysis done by Quan,(ref 2), this simplification is valid and acceptable. We assume that the elastic moduli in the direction along the fiber axis is equal for both the radial and circumferential bundles. Table (1) shows the difference to be only eight percent.

$$(E_{rr})_a = (E_{\theta\theta})_a = E$$

The circumference of the billet is $C = 2\pi r$. When the

billet is rapidly heated, both the inner and outer dimensions will change.

The outer circumference, Co′ can be expressed as:

$$C_o' = C_o + \Delta C_o = C_o + C_o\varepsilon_m + C_o\alpha\Delta T \qquad \text{A-1}$$

Where ε_m is the mechanical strain.

$$2\,R_o' = 2\pi R_o + 2\pi R_o \frac{\sigma_{\theta\theta}}{E} + 2\pi R_o\alpha\Delta T \qquad \text{A-2}$$

$$R_o' = R_o\left[1 + \frac{\sigma_{\theta\theta}}{E} + \alpha\Delta T\right] \qquad \text{A-3}$$

Where α is the coefficient of thermal expansion, R is the original billet radius, and R′ is the billet radius immediately after rapid heat up.

Similarly, the inner radius will be;

$$R_i' = R_i\left[1 + \frac{\sigma_{\theta\theta}}{E} + \alpha\Delta T\right] \qquad \text{A-4}$$

The mechanical strain in the radial direction is given by:

$$\varepsilon_{rr} = \left[\frac{(R_o' - R_i') - (R_o - R_i)}{(R_o - R_i)} \right] - \alpha \Delta T \qquad A-5$$

Combining with equations A-3 and A-4

$$\varepsilon_{rr} = \left[\frac{R_o + R_i}{R_o - R_i} \right] \frac{\sigma_{\theta\theta}}{E} \qquad A-6$$

This is the maximum mechanical strain that a radial bundle will experience, if perfect bonding exists between the radials and the corresponding matrix.

The stress in the radial bundle can be given by;

$$\sigma_{rr} = E_{rr}\, \varepsilon_{rr} = E_{rr} \left[\frac{\sigma_{\theta\theta}}{E_{\theta\theta}} \right] \left[\frac{R_o + R_i}{R_o - R_i} \right] \qquad A-7$$

Finally, the stress in the radial fibers can be expressed as:

$$\sigma_{rr} = \sigma_{\theta\theta} \left[\frac{R_o + R_i}{R_o - R_i} \right] \qquad A-8$$

From the above analysis, one can see that the stress in

the radial bundles is always greater than that of the circumferential bundles. Variations in the stress along the radial bundles will result in a peak stress higher than this average value.

The above model considered the bundles isolated from the composite without direct interaction with the local thermal expansion of the composite. Julius Jortner (3) recently made a second order approximation which gives;

$$\frac{B\bar{\varepsilon}_r}{B\bar{\varepsilon}_\theta} \quad \frac{C^*_{\varepsilon_\theta}\,\frac{(R_o + R_i)}{(R_o - R_i)} + (C_{\alpha_\theta} - B_\alpha)\,\Delta T}{C^*_{\varepsilon_A} + (C_{\alpha_A} - B_\alpha)\,\Delta T}$$

Where;

$B\bar{\varepsilon}_r$	Average axial mechanical strain in the radial bundle.
$B^*_{\varepsilon_\theta}$	Axial tensile mechanical strain in the radial bundle at the outer radius Ro, (it is assumed to be approximately equal in magnitude to the compressive strain in the circumferential bundle at the inner radius Ri).
$C^*_{\varepsilon_\theta}$	Mechanical circumferential strain in the composite at Ro.
C_{α_θ}	Coefficient of thermal expansion of the bundle.
B_α	Axial coefficient of thermal expansion of the bundle.

Notice that this analysis also predicts that the strain (stress) in the radial bundles is always higher than the peak strain (stress) in the circumferential bundles.

Both models are limited to giving the average of the

axial mechanical strain in the radial bundles; it will be seen that the peak strain in the radial bundles will be higher: The radial composite stress (strain) which occurs upon heating is compressive while being zero at the outer and inner radii and has a roughly parabolic shape with the peak near the middle of the radial thickness. Shear interaction of the radial bundles with this compressive composite strain would decrease the axial tensile stress in the radial bundles would be higher near the outer and inner radii and higher than the average predicted by both of the above analyses. (Jortner considers the above in a quantitative way in the draft of his report in preparation.)

Many billets have a layered structure where the number of radial fibers is increased at the outer radius in an attempt to make the radial bundle density more constant. Neither analysis considers this effect or the coincident effect of termination of some fibers at the layered interfaces.

APPENDIX B

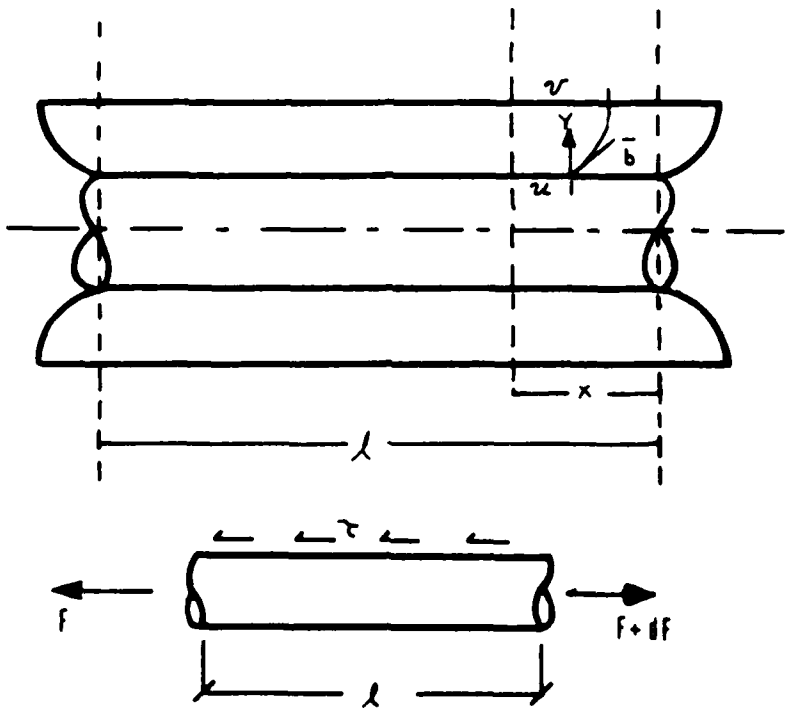

Force Equilibrium

$$(F + dF) - F - 2\pi r\, \tau dx = 0$$

$$dF = 2\pi r\, \tau dx$$

Displacement of fiber to matrix is (v-u).

b is the effective thickness of the bundle matrix interface, where at Y=0, $\mathcal{U}$ =max, and at Y=b, V =0

The shear strain $\gamma = \frac{v - u}{b}$ B-3

Shear modulus $= G_m$

Therefore: $\gamma = \frac{\tau}{G}$ B-4

Combining equations (2), (3), and (4)

$$v - u = \left(\frac{b}{G}\right)\left(\frac{1}{2\pi r}\right)\left(\frac{dF}{dx}\right) \quad \text{B-5}$$

Differentiating

$$\frac{dv}{dx} - \frac{du}{dx} = \left(\frac{b}{G}\right)\left(\frac{1}{2\pi r}\right)\left(\frac{d^2F}{dx^2}\right) \quad \text{B-6}$$

Since the strain in the matrix is:

$$\frac{dv}{dx} = \varepsilon_m \quad \text{B-7}$$

and

$$\frac{du}{dx} = \varepsilon_f = \left(\frac{F}{\pi r^2}\right)\left(\frac{1}{E_f}\right) \quad \text{B-8}$$

Combining (7) and (8) into (6) gives;

$$\frac{d^2F}{dx^2} = \frac{2\pi rG_m}{b}\left[\frac{\partial v}{\partial x} - \frac{\partial u}{\partial x}\right] = \frac{2\pi rG_m}{b}\left[\epsilon_m - \frac{F}{r^2E_f}\right] \qquad B-9$$

Letting

$$\alpha = \left[\frac{2G_m}{brE_f}\right]^{\frac{1}{2}} \qquad B-10$$

$$\frac{d^2F}{dx^2} = -\alpha^2F + \alpha^2(E_f\pi r^2\epsilon_m)$$

$$F'' + \alpha^2F - \alpha^2(E_f\pi r^2\epsilon_m) = 0 \qquad B-11$$

The solution of this equation is in the form:

$$F = E_f\pi r^2\epsilon_m + C_1\sinh(\alpha x) + C_2\cosh(\alpha x) \qquad B-12$$

By inserting the appropriate boundary conditions the constants can be found for specific cases.

APPENDIX C

DATA TABLES FOR PULL-OUT SPECIMENS

DATA TABLE FOR AXIAL PULL-OUT SPECIMENS

SPECIMEN	GAGE LENGTH (IN)	FIBER DIMENSIONS (AxB) (in)	TEMP (C)	BREAK-FREE LOAD (lb)	FRICTION LOAD (lb)
A-5	0.424	.051 X .045	ROOM	85	-
A-6	0.386	.038 X .055	ROOM	63	-
A-7	0.333	.049 X .052	ROOM	73	-
A-8	0.345	.045 X .062	ROOM	51	-
A-9	0.225	.052 X .058	1000	65	-
A-10	0.332	.035 X .051	1500	90	72
A-11	0.300	.050 X .034	ROOM	60	54
A-12	0.305	.045 X .060	1000	66	53
A-13	0.296	.053 X .057	ROOM	60	60
A-14	0.304	.044 X .050	ROOM	66	24
A-15	0.310	.044 X .030	1000	80	48
A-16	0.260	.047 X .049	1500	78	63
A-17	0.303	.050 X .060	1500	108	87
A-18	0.300	.057 X .045	1000	67	57

DATA FOR RADIAL PULL-OUT SPECIMENS

SPECIMEN	GAGE LENGTH (IN)	FIBER DIMENSIONS (AxB) (IN)	TEMP (C)	BREAK-FREE LOAD (lb)	FRICTION LOAD (lb)
R-5	0.386	.020 X .031	1000	41	22
R-6	0.375	.021 X .032	1000	52	31
R-7	0.404	.020 X .029	1500	43	18
R-8	0.403	.021 X .031	ROOM	33	23
R-9	0.382	.022 X .030	1500	30	-
R-10	0.313	.028 X .020	1500	51	20
R-11	0.307	.031 X .031	1500	54	-
R-12	0.300	.021 X .031	1000	36	18
R-13	0.313	.030 X .035	1500	35	20
R-14	0.253	.035 X .041	ROOM	63	48
R-15	0.330	.020 X .031	ROOM	42	21
R-16	0.350	.020 X .036	1500	45	33
R-17	0.323	.022 X .037	ROOM	33	33
R-18	0.324	.019 X .031	1000	39	29

APPENDIX D

DATA FOR AXIAL RUPTURE SPECIMENS

Eleven specimens were tested at room temperature for axial rupture at three different stages of processing. Seven specimens were tested after the impregnation stage, three specimens tested after the calcination stage, and one specimen tested after the graphitization stage. The cross-sectional area used in the calculation of the rupture stress is based on the dry fiber bundle area only. The fiber bundle area was found in two ways: The first was to weigh a three foot piece of a dry HM3000 fiber bundle which comprises 3000 fibers, then, knowing the density from the manufacturer's data, calculated the filament diameter which was 6.8μm (2.68×10^{-4} in). The second method of finding the filament diameter was to isolate a single filament under a microscope and take a photomicrograph of it, along with an objective micrometer. The objective micrometer had divisions of 1μm, therefore only an approximation could be made at 7μm, (2.76×10^{-4} in). For the purpose of this paper, the filament diameter of 6.8μm, (2.68×10^{-4} in) was used thus giving a dry fiber bundle area of 1.69×10^{-4} in^2. The results of the eleven rupture tests are shown below.

SPECIMEN	LOAD (lb)	STRESS IMPREGNATED (ksi)	CALCINED (ksi)	GRAPHITIZED (ksi)
1	34	201.4	-	-
2	41	242.8	-	-
3	38	-	225.0	-
4	33	195.4	-	-
5	44	260.6	-	-
6	41	-	242.8	-
7	35	207.3	-	-
8	40	-	-	236.9
9	37	219.1	-	-
10	37	-	219.1	-
11	42	248.7	-	-
Average		225.0	228.9	236.9
Std. Deviation		25.58	12.34	-

Note: Although the data shows a small increase in the average strength of the specimens with the higher stages of processing, the variation in data is large enough that we cannot definitely conclude that the bundle strength increases with processing, because of the small number of samples tested.

ORGANIZATION	LASTNAME	FIRSTNAME	CITY	STATE	ZIPCODE
ACUREX/AEROTHERM	Carlson	D. L.	Mountain View	CA	94042
ACUREX/AEROTHERM	Zimmer	J. E.	Mountain View	CA	94042
AEROJET ELECTROSYSTEMS	Buch	J. D.	Azusa	CA	91702
AEROJET STRATEGIC PROPULSION COMPANY	Davis	H. O.	Sacramento	CA	95813
AEROJET STRATEGIC PROPULSION COMPANY	Marchol	P.	Sacramento	CA	95813
AERONUTRONIC FORD	Pope	J.	Newport Beach	CA	92663
AEROSPACE CORPORATION	Baker	R. L.	Los Angeles	CA	90009
AEROSPACE CORPORATION	Chase	A. B.	Los Angeles	CA	90009
AEROSPACE CORPORATION	Evangelides	J. S.	Los Angeles	CA	90009
AEROSPACE CORPORATION	Feldman	L.	Los Angeles	CA	90009
AEROSPACE CORPORATION	Meyer	Robert A.	Los Angeles	CA	90009
AEROSPACE CORPORATION	Robinson	E. Y.	Los Angeles	CA	90009
AEROSPACE CORPORATION	Rubin	L.	Los Angeles	CA	90009
AEROSPACE CORPORATION	White	J. L.	Los Angeles	CA	90009
AFOSR/NC	Ulrich	D. R.	Bolling AFB	DC	20332
AFWAL/MLBC	Abrams	Frances	Wright-Patterson AFB	OH	45433
AFWAL/MLBC	Schmidt	D.	Wright-Patterson AFB	OH	45433
AFWAL/MLBC	Theibert	L. Scott	Wright-Patterson AFB	OH	45433
AFWAL/MLBE	Craig	R. E.	Wright-Patterson AFB	OH	45433
AFWAL/MLBL	Kessler	W. C.	Wright-Patterson AFB	OH	45433
AFWAL/MLBM	Drzal	L. T.	Wright-Patterson AFB	OH	45433
AFWAL/MLBM	Pagano	N. J.	Wright-Patterson AFB	OH	45433
AFWAL/MLLM	Graham	H. C.	Wright-Patterson AFB	OH	45433
AFWAL/MLLM	Kerans	R.	Wright-Patterson AFB	OH	45433
AFWAL/MS	Tallan	N. M.	Wright-Patterson AFB	OH	45433
AFWL/NTY	**********		Kirtland AFB	NM	87117
AIR FORCE ROCKET PROPULSION LABORATORY	Ismael	I.	Edwards AFB	CA	93523
AIR FORCE ROCKET PROPULSION LABORATORY	Tepe	L.	Edwards AFB	CA	93523
ARMY MATERIALS & MECHANICS RES. CENTER	Uhlir	D.	Watertown	MA	02172
ARMY RESEARCH OFFICE	Meyer	George	Research Triangle Pk	NC	27709
ATLANTIC RESEARCH CORPORATION	Baetz	J.	Alexandria	VA	22314
ATLANTIC RESEARCH CORPORATION	Frankle	R. S.	Alexandria	VA	22314
AVCO Corporation	Laskaris	T.	Lowell	MA	01851
AVCO Corporation	Rolincik	P.	Wilmington	MA	01887
AVCO Systems Division	Taverna	Art	Wilmington	MA	01887
B.F. GOODRICH R&D CENTER	Stover	E.	Brecksville	OH	44191
BATTELLE COLUMBUS LABORATORIES	Jelinek	Frank J.	Columbus	Ohio	43201
CALIFORNIA RESEARCH & TECHNOLOGY, INC.	Kreyenhagen	K. N.	Chatsworth	CA	91311
DEFENSE NUCLEAR AGENCY	Kohler	D.	Washington	DC	20305
DEFENSE TECHNICAL INFORMATION CENTER	**********		Alexandria	VA	22314
DEPARTMENT OF THE NAVY	Crone	J.	Washington	DC	20360
EFFECTS TECHNOLOGY, INC.	Adler	M.	Santa Barbara	CA	93105
EFFECTS TECHNOLOGY, INC.	Graham	M.	Santa Barbara	CA	93105
EIXON ENTERPRISES, INC.	Riggs	D.	Fountain Inn	SC	29644
FIBER MATERIALS, INC.	Lander	L. L.	Biddeford	ME	04005
FIBER MATERIALS, INC.	McAllister	L.	Biddeford	ME	04005
GA Technologies	Engle	Glen B.	San Diego	CA	92138
GENERAL ELECTRIC COMPANY	Franke	Robert	Cincinnati	OH	45215
GENERAL ELECTRIC COMPANY	Hall	Kenneth J.	Philadelphia	PA	19101
GENERAL ELECTRIC SPACE DIVISION -RSO	Gebhardt	J.	Philadelphia	PA	19101
HAVE6	Pegg	R.	Santa Fe Springs	CA	90670
HERCULES CORPORATION	Christensen	P.	Magna	UT	84044

ORGANIZATION	LASTNAME	FIRSTNAME	CITY	STATE	ZIPCODE
HITCO	Dyson	L.	Gardena	CA	90249
IIT Research Institute	Larsen	D. C.	Chicago	Illinois	60616
JET PROPULSION LABORATORY	Kimmel	M.	Pasadena	CA	91103
JORTNER RESEARCH & ENGINEERING, INC.	Jortner	Julius	Costa Mesa	CA	92628
KAISER	Fischer	M.	San Leandro	CA	94577
LAWRENCE LIVERMORE LABORATORIES	Maimoni	A.	Livermore	CA	94550
LOCKHEED MISSILES & SPACE COMPANY, INC.	Pinoli	Pat C.	Palo Alto	CA	94304
LOCKHEED MISSILES AND SPACE COMPANY	Osaka	M.	Sunnyvale	CA	94088
MARTIN MARIETTA AEROSPACE	Koo	F. H.	Orlando	FL	32855
MASSACHUSETTS INSTITUTE OF TECHNOLOGY	Uhlman	D. R.	Cambridge	MA	02139
MATERIALS SCIENCES CORPORATION	Kibler	J. J.	Springhouse	PA	19477
MATERIALS SCIENCES CORPORATION	Rosen	B. Walter	Springhouse	PA	19477
MCDONNELL DOUGLAS ASTRONAUTICS CO.	Greszczuk	L. B.	Huntington Beach	CA	92647
MCDONNELL DOUGLAS ASTRONAUTICS CO.	Penton	A. P.	Huntington Beach	CA	92647
MCDONNELL DOUGLAS RESEARCH LABORATORY	Holman	M.	St. Louis	MO	63166
NASA Lewis	Grimes	H.	Cleveland	OH	44135
NASA Langley	Houston	R. J.	Langley	VA	23665
NASA Langley	Rummler	D.	Langley	VA	23665
NASA Langley	Sawyer	J. W.	Langley	VA	23665
NASA Marshall Space Flight Center	Powers	B.	Huntsville	AL	35812
NAVAL RESEARCH LABORATORY	**********		Washington	DC	20375
NAVAL SEA SYSTEMS COMMAND	Kinna	M.	Washington	DC	20302
NAVAL WEAPONS CENTER	Jeter	Edward	China Lake	CA	93555
NSWC/WOL	Koubek	F. J.	Silver Spring	MD	20910
NSWC/WOL	Rowe	Charles R.	Silver Spring	MD	20910
OFFICE OF NAVAL RESEARCH	**********		Pasadena	CA	91106
OFFICE OF NAVAL RESEARCH	Diness	A. M.	Arlington	VA	22217
OFFICE OF NAVAL RESEARCH	Kushner	A. S.	Arlington	VA	22217
OFFICE OF NAVAL RESEARCH	Peebles	L. H.	Arlington	VA	22217
OSD/DDR&E	Persh	J.	Washington	DC	20301
PDA Engineering	Crose	J. G.	Santa Ana	CA	92705
PDA Engineering	Mack	T. E.	Santa Ana	CA	92705
PDA Engineering	Stanton	E. L.	Santa Ana	CA	92705
PICATINNY ARSENAL	Anazione	A.	Dover	NJ	07801
PRATT & WHITNEY AIRCRAFT	Miller	Robert L.	West Palm Beach	FL	33402
PRATT & WHITNEY AIRCRAFT	Schmid	Tom	West Palm Beach	FL	33402
PURDUE UNIVERSITY	Sun	C. T.	West Lafayette	IN	47907
PURDUE UNIVERSITY	Taylor	R. E.	West Lafayette	Indiana	47906
RENSSELAER POLYTECHNIC INSTITUTE	Diefendorf	R. J.	Troy	NY	12181
ROCKETDYNE DIVISION, ROCKWELL INTERNTL	Hawkinson	E. L.	Canoga Park	CA	91304
SAMSO/MNNR	Bailey	D.	Norton AFB	CA	92409
SAMSO MNNR	Brocato	T.	Norton AFB	CA	92409
SANDIA LABORATORIES	Northrup	D.	Albuquerque	NM	87185
SCIENCE APPLICATIONS, INC.	Eitman	D.	Irvine	CA	92715
SCIENCE APPLICATIONS, INC.	Loomis	Willard	Irvine	CA	92715
SOUTHERN RESEARCH INSTITUTE	Koenig	John	Birmingham	AL	35205
SOUTHERN RESEARCH INSTITUTE	Pears	C.	Birmingham	AL	35205
SOUTHERN RESEARCH INSTITUTE	Starrett	H. Stuart	Birmingham	AL	35205
SOUTHWEST RESEARCH INSTITUTE	Lankford	J.	San Antonio	TX	78284
STACKPOLE FIBERS COMPANY, INC.	Fleming	G.	Lowell	MA	01852
STRATEGIC SYSTEMS PROJECT OFFICE (PM-1)	Kincaid	J.	Washington	DC	20376

ORGANIZATION	LASTNAME	FIRSTNAME	CITY	STATE	ZIPCODE
STRATEGIC SYSTEMS PROJECT OFFICE (PM-1)	Weinger	S.	Washington	DC	20376
SUPERTEMP CENTER	Leeds	Don	Santa Fe Springs	CA	90670
SYSTEMS, SCIENCE AND SOFTWARE	Gurtman	G.	La Jolla	CA	92037
THIOKOL	Broman	G.	Brigham City	UT	84302
TRW Systems	Kotlensky	Wm.	San Bernardino	CA	92402
U.S. ENERGY RESEARCH DIV. ADMINISTRATION	Littman	A.	Washington	DC	20331
UNION CARBIDE CORPORATION	Bowman	J.	Cleveland	OH	44101
UNION CARBIDE CORPORATION	Taylor	A.	Oak Ridge	TN	37839
UNITED TECHNOLOGIES RESEARCH CENTER	Gallaso	F.	Hartford	CT	06100
UNITED TECHNOLOGIES-CSD	Ellis	Russ	Sunnyvale	CA	94088
UNIVERSITY OF CALIFORNIA	Batdorf	S. B.	Los Angeles	CA	90024
UNIVERSITY OF CALIFORNIA	Sines	George	Los Angeles	CA	90024
UNIVERSITY OF WASHINGTON	Fischbach	D.	Seattle	WA	98195
UNIVERSITY OF WYOMING	Adams	D. F.	Laramie	WY	82071
VIRGINIA POLYTECHNIC INSTITUTE	Hasselman	D. P. H.	Blacksburg	VA	24061
VIRGINIA POLYTECHNIC INSTITUTE	Jones	Robert M.	Blacksburg	VA	24061
VOUGHT CORPORATION	Volk	H.	Dallas	TX	75211
WILLIAMS INTERNATIONAL	Cruzen	Scott	Walled Lake	MI	48088

END

FILMED

8-85

DTIC